

Light propagation and gravitational lensing on the Weyl-like spacetime in scalar-tensor theories of gravity

Shin-ei TSUNEISHI¹ *) , Kazuya WATANABE² **)
and Tooru TSUCHIDA³ ***)

¹ *Graduate School of Science and Technology, Niigata University Niigata,
950-2181, Japan*

² *Department of Physics, Niigata University, Niigata 950-2181, Japan*

³ *Kokugakuin University Tochigi High School, Tochigi 328-8588, Japan.*

We study light propagation and gravitational lensing in scalar-tensor theories of gravity by using a static, axisymmetric exterior solution. The solution, which has been studied by Tsuchida and Watanabe, has asymptotic flatness properties and moreover is reduced to Voorhees's one of Weyl's series of prolate solutions in the case of a constant scalar field. We first obtain an asymptotic form of the solution near the spatial infinity in order to clarify the physical significance of three model parameters found in the solution. It is shown that an amplitude of the scalar field, a non-sphericity of the spacetime symmetry and a mass-like parameter in the Einstein frame are represented in terms of these three parameters. As for the spacetime structure, we also give brief discussion on the directional-dependent properties of the spacetime singularity. We then study null geodesic equations and Sachs's optical scalar equations on the equatorial plane in order to investigate deflection and shear of light rays. Our studies are done by using a technique of the conformal transformation such that their results are independent of details of scalar-tensor theories of gravity owing to the conformally invariant properties of null geodesics. For some specific values of the model parameters, we analytically obtain a deflection angle of the light path and find that it can become negative. The appearance of a negative deflection angle indicates "reflection" of a light path, and we investigate under which conditions the light reflection occurs. As for the optical scalars, we find that the Weyl source-term shows significantly different properties when it is compared with that in the Schwarzschild spacetime. We therefore classify a space of the model parameters into four distinct regions on the basis of the qualitative properties of the Weyl source-term and find a close relationship between this classification of the parameter space and the occurrence of the light reflection. We finally solve the null geodesic equations and the optical scalar equations numerically. We find that a picture of the thin lens is applicable and give a simple analytic model for the optical scalars. As for the properties of gravitational lensing, the deflection angle and the image distortion rate are obtained as functions of the impact parameter. Again, we find a close relationship between their qualitative properties and the classification above.

§1. Introduction

Scalar-tensor theories of gravity have been studied by many theoretical physicists

*) tuneishi@astro.sc.niigata-u.ac.jp

**) kazuya@astro.sc.niigata-u.ac.jp

***) CZL03253@nifty.ne.jp

as natural alternatives to general relativity since the pioneering work by Brans and Dicke.¹⁾ In particular, a theory of dilaton gravity has been of interest as an effective theory of the superstring theories at low energy scales.²⁾ In these theories, the gravity is mediated not only by a tensor field but also by a scalar field. Several theoretical predictions in the scalar-tensor theories have been obtained,^{3)–7)} and it has been found that a wide class of the scalar-tensor theories can pass all the experimental tests in the cases of weak gravitational fields. In the cases of strong gravitational fields, however, it has been found that the scalar-tensor theories show different aspects of the gravity in contrast to general relativity. For example, it has been shown numerically that nonperturbative effects in the scalar-tensor theories increase the maximum mass of an isolated system such as a neutron star.^{3)–5)} In these works, numerical methods play an important role, and a spherical exterior solution, which is a static, spherically symmetric exterior solution outside a spherical body, is matched to the numerical solution in interpreting its results. A usual astronomical object, however, has a non-spherical form and is in rotation, and not only a spherical exterior solution but also axisymmetric exterior solutions may therefore play an important role in discussing the crucial difference between general relativity and scalar-tensor theories of gravity.

Among the axisymmetric exterior solutions, ones corresponding to the series of solutions of Tomimatsu and Sato in general relativity⁸⁾ must be of significant interest. It is, however, difficult to obtain their explicit forms, and the case is similar even for solutions corresponding to Kerr's solution in general relativity. Instead of studying such the Kerr-like solutions, Tsuchida and Watanabe⁷⁾ have investigated the Weyl-like solutions, namely the solutions which are reduced to those of Weyl's series in the case of a constant scalar field. Among these Weyl-like solutions, we have a special solution, which we shall refer to as the scalar-tensor-Weyl solution. This solution is very notable for the reason that it has asymptotic flatness properties and moreover is reduced to Voorhees's solution,⁹⁾ namely a solution of Weyl's series of prolate solutions, in the case of a constant scalar field. Several geometrical properties of the scalar-tensor-Weyl solution, especially the properties of light propagation, have been investigated by analytical approaches in Ref.7. On the basis of this work, we will study light propagation and gravitational lensing on the scalar-tensor-Weyl solution by numerical approaches because the local properties of null geodesics must tell us important geometrical information of the spacetime.

In this paper, we first study the global structure of the scalar-tensor-Weyl solution. We obtain an asymptotic form of the solution near the spatial infinity in order to clarify the physical significance of three model parameters found in the solution. It may be interesting that the Schwarzschild-like coordinates can be naturally introduced in doing that. It will be shown that these parameters are related to an amplitude of the scalar field, a non-sphericity of the spacetime symmetry and a mass-like parameter in the Einstein frame. The directional-dependent properties of the spacetime singularity will be also shown. After giving the several analytical results as briefly summarized in Abstract, we numerically solve null geodesic equations and Sachs's optical scalar equations.¹⁰⁾ By using a technique of the conformal transformation, we then study deflection and shear of light rays on the equatorial

plane in the manner such that the obtained results are independent of details of scalar-tensor theories of gravity. We numerically obtain the deflection angle and the image distortion rate as functions of the impact parameter and find a close relationship between their qualitative properties and the classification of the model parameter space according to the Weyl source-term. Several analytic results shown in the previous papers are summarized in Appendices.^{7),11)}

Throughout this paper, we use the system of units such that $c = G = 1$.

§2. The scalar-tensor-theory of gravity

We consider the simplest scalar-tensor theory in which gravitational interactions are mediated by a tensor field, $\hat{g}_{\mu\nu}$, and a scalar field, $\hat{\phi}$.^{1),3)-7)} Hereafter, a hat ($\hat{\quad}$) is used to denote quantities and derivatives associated with $\hat{g}_{\mu\nu}$. An action of the theory is given as

$$S = \frac{1}{16\pi} \int \left[\hat{\phi} \hat{R} - \frac{\omega(\hat{\phi})}{\hat{\phi}} \hat{g}^{\mu\nu} \hat{\phi}_{,\mu} \hat{\phi}_{,\nu} \right] \sqrt{-\hat{g}} d^4x + S_{\text{matter}}[\hat{\Psi}_m, \hat{g}_{\mu\nu}], \quad \hat{\phi}_{,\mu} \equiv \frac{\partial \hat{\phi}}{\partial x^\mu}, \quad (2.1)$$

where $\omega(\hat{\phi})$ is a dimensionless function of $\hat{\phi}$ and specifies the theory, $\hat{\Psi}_m$ represents matter fields, and S_{matter} is an action of the matter fields. The scalar field, $\hat{\phi}$, plays the role of an effective gravitational constant, \hat{G} , as $\hat{G} \sim 1/\hat{\phi}$. Varying the action by the tensor field, $\hat{g}_{\mu\nu}$, and the scalar field, $\hat{\phi}$, yields, respectively, the following field equations,

$$\begin{aligned} \hat{G}_{\mu\nu} &= \frac{8\pi}{\hat{\phi}} \hat{T}_{\mu\nu} + \frac{\omega(\hat{\phi})}{\hat{\phi}^2} \left(\hat{\phi}_{,\mu} \hat{\phi}_{,\nu} - \frac{1}{2} \hat{g}_{\mu\nu} \hat{g}^{\alpha\beta} \hat{\phi}_{,\alpha} \hat{\phi}_{,\beta} \right) \\ &\quad + \frac{1}{\hat{\phi}} (\hat{\nabla}_\mu \hat{\phi}_{,\nu} - \hat{g}_{\mu\nu} \hat{\nabla}^\alpha \hat{\phi}_{,\alpha}), \end{aligned} \quad (2.2)$$

$$\hat{\nabla}^\alpha \hat{\phi}_{,\alpha} = \frac{1}{3 + 2\omega(\hat{\phi})} \left(8\pi \hat{T} - \frac{d\omega(\hat{\phi})}{d\hat{\phi}} \hat{g}^{\alpha\beta} \hat{\phi}_{,\alpha} \hat{\phi}_{,\beta} \right), \quad (2.3)$$

where $\hat{\nabla}_\alpha$ and $\hat{T}_{\mu\nu}$ denote, respectively, a covariant derivative and an energy-momentum tensor associated with $\hat{g}_{\mu\nu}$. Now we perform the following conformal transformation to a new frame called the Einstein frame with the metric, $g_{\mu\nu}$, defined by

$$g_{\mu\nu} = A^{-2}(\varphi) \hat{g}_{\mu\nu}, \quad (2.4)$$

such that

$$A^2(\varphi) = \frac{1}{\hat{\phi}}, \quad \frac{1}{3 + 2\omega(\hat{\phi})} = \left(\frac{d \ln A(\varphi)}{d\varphi} \right)^2 \equiv \alpha^2(\varphi), \quad (2.5)$$

where $A(\varphi)$ and $\alpha(\varphi)$ are referred to as a coupling function and a coupling strength, respectively. Then the action is rewritten as

$$S = \frac{1}{16\pi} \int (R - 2g^{\mu\nu} \varphi_{,\mu} \varphi_{,\nu}) \sqrt{-g} d^4x + S_{\text{matter}}[\hat{\Psi}_m, A^2(\varphi) g_{\mu\nu}]. \quad (2.6)$$

Varying the action by $g_{\mu\nu}$ and φ yields, respectively,

$$G_{\mu\nu} = 8\pi T_{\mu\nu} + 2 \left(\varphi_{,\mu} \varphi_{,\nu} - \frac{1}{2} g_{\mu\nu} g^{\alpha\beta} \varphi_{,\alpha} \varphi_{,\beta} \right), \quad (2.7)$$

$$\nabla^\mu \varphi_{,\mu} = -4\pi \alpha(\varphi) T, \quad (2.8)$$

where ∇_α and $T_{\mu\nu}$ denote, respectively, a covariant derivative and an energy-momentum tensor associated with $g_{\mu\nu}$. A relationship between $T^{\mu\nu}$ and $\hat{T}^{\mu\nu}$ is given by

$$T^{\mu\nu} \equiv \frac{2}{\sqrt{-g}} \frac{\delta S_{\text{matter}}[\hat{\Psi}_m, A^2(\varphi)g_{\mu\nu}]}{\delta g_{\mu\nu}} = A^6(\varphi) \hat{T}^{\mu\nu}. \quad (2.9)$$

The conservation law for $T^{\mu\nu}$ is given by

$$\nabla_\nu T^{\mu\nu} = \alpha(\varphi) T \nabla^\mu \varphi. \quad (2.10)$$

§3. Geometrical properties of the scalar-tensor-Weyl solution

We investigate the geometrical properties of the scalar-tensor-Weyl solution.⁷⁾ The reduced field equations and the derivation of the solution are given in Appendices A and B.

3.1. The scalar-tensor-Weyl solution

The scalar-tensor-Weyl solution is one of the static, axisymmetric vacuum solutions in the Einstein frame with the metric,

$$ds^2 = - \left(\frac{x-1}{x+1} \right)^\delta dt^2 + \sigma^2 \left(\frac{x-1}{x+1} \right)^{-\delta} \times \left[\left(\frac{x^2-1}{x^2-y^2} \right)^{\Delta^2} (x^2-y^2) \left(\frac{dx^2}{x^2-1} + \frac{dy^2}{1-y^2} \right) + (x^2-1)(1-y^2)d\phi^2 \right], \quad (3.1)$$

and the scalar field,

$$\varphi = \varphi_0 + \frac{d}{2} \ln \left(\frac{x-1}{x+1} \right), \quad (3.2)$$

where a positive constant, σ , is a unit of length, and δ , φ_0 and d are integration constants. A parameter, Δ , is defined by

$$\Delta^2 \equiv \delta^2 + d^2, \quad \Delta \geq 0. \quad (3.3)$$

Now we show that the above solution is reduced to the previously known ones when we take specific values of the parameters, δ and Δ . When $\Delta = \delta$, i.e., $d = 0$, the

metric is reduced to Voorhees's prolate solution⁹⁾ which is one of Weyl's series of the solutions in general relativity. Voorhees's prolate solution contains the Schwarzschild solution as a specific case, $\delta = 1$, and the Schwarzschild coordinates are related to the coordinates, x and y , as

$$x = \frac{r}{\sigma} - 1, \quad y = \cos \theta, \quad m = \sigma, \quad (3.4)$$

where m plays the role of a usual mass parameter of the Schwarzschild spacetime.

When $\Delta = 1$, we introduce the Just coordinates by

$$x = \frac{\chi}{\sigma} - 1, \quad y = \cos \theta, \quad m = \delta\sigma. \quad (3.5)$$

Then (3.1) is reduced to a spherical exterior solution,

$$ds^2 = - \left(1 - \frac{2m}{\delta\chi}\right)^\delta dt^2 + \left(1 - \frac{2m}{\delta\chi}\right)^{-\delta} d\chi^2 + \chi^2 \left(1 - \frac{2m}{\delta\chi}\right)^{1-\delta} (d\theta^2 + \sin^2 \theta d\phi^2). \quad (3.6)$$

This result tells us that the parameter, Δ , has the physical significance of a non-sphericality of the spacetime symmetry. The Schwarzschild coordinate, r , is related to the Just coordinate, χ , as

$$r = \chi \left(1 - \frac{2m}{\delta\chi}\right)^{\frac{1-\delta}{2}}. \quad (3.7)$$

When $\Delta = \delta = 1$, the spherical exterior solution (3.6) is reduced to Schwarzschild's one, and, in this case, the scalar field becomes a constant. A relationship among these solutions is shown in Figure 1.

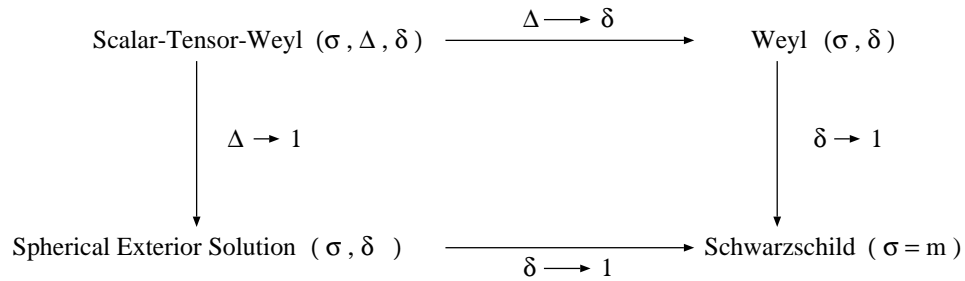


Fig. 1. A schematic depiction of series of the scalar-tensor-Weyl solutions.

3.2. An asymptotic form of the scalar-tensor-Weyl solution near the spatial infinity

Now, in order to clarify the physical significance of the parameters, Δ and δ , we study an asymptotic form of the scalar-tensor-Weyl solution near the spatial infinity. We first define the asymptotically Schwarzschild-like coordinates, (r, θ) , by

$$x = \frac{\Delta}{\sqrt{2}} \left[u^2 + v^2 + \frac{1 - \Delta^2}{\Delta^2} + \sqrt{\left(u^2 + v^2 + \frac{1 - \Delta^2}{\Delta^2} \right)^2 - \frac{4u^2v^2}{\Delta^2}} \right]^{\frac{1}{2}}, \quad (3.8)$$

$$y = \pm \frac{\Delta}{\sqrt{2}} \left[u^2 + v^2 + \frac{1 - \Delta^2}{\Delta^2} - \sqrt{\left(u^2 + v^2 + \frac{1 - \Delta^2}{\Delta^2} \right)^2 - \frac{4u^2v^2}{\Delta^2}} \right]^{\frac{1}{2}}, \quad (3.9)$$

$$u = \frac{\delta}{m\Delta} \chi - 1, \quad v = \cos \theta, \quad m = \delta \sigma, \quad (3.10)$$

$$\frac{m}{\chi} = \frac{m}{r} + \left(1 - \frac{\Delta}{\delta} \right) \left\{ \frac{m^2}{r^2} + \left(3 - \frac{\Delta}{\delta} \right) \frac{m^3}{2r^3} \right\}, \quad (3.11)$$

which are reduced to (3.5) when $\Delta = 1$. The equations in the above complicated forms are obtained under the following requirements.

- (a) The equations (3.8) and (3.9) are the same as those in Voorhees's prolate solution, and one has $\chi = r$ for $\Delta = \delta$ such that the asymptotic form of the solution becomes that of Voorhees's one.⁹⁾ In particular, an asymptotic form of g_{tt} for $\Delta = \delta$ becomes

$$g_{tt} = -1 + \frac{2m}{r} - \frac{2}{3} \left(\frac{\delta^2 - 1}{\delta^2} \right) \left(\frac{3}{2} \cos^2 \theta - \frac{1}{2} \right) \frac{m^3}{r^3} + \mathcal{O} \left(\frac{m^4}{r^4} \right). \quad (3.12)$$

- (b) When $\Delta = 1$, the asymptotic form of the solution is the same as that of the spherical exterior solution, and an asymptotic form of g_{tt} and the relation between the Schwarzschild coordinate, r , and the Just coordinate, χ , are, respectively, given by

$$g_{tt} = -1 + \frac{2m}{r} + \frac{1}{3} \left(1 - \frac{1}{\delta^2} \right) \frac{m^3}{r^3} + \mathcal{O} \left(\frac{m^4}{r^4} \right), \quad (3.13)$$

$$\frac{m}{\chi} = \frac{m}{r} + \left(1 - \frac{1}{\delta} \right) \left\{ \frac{m^2}{r^2} + \left(3 - \frac{1}{\delta} \right) \frac{m^3}{2r^3} + \mathcal{O} \left(\frac{m^4}{r^4} \right) \right\}. \quad (3.14)$$

- (c) For any values of Δ and δ , asymptotic forms of g_{tt} and $g_{\theta\theta}$ become, respectively,

$$g_{\theta\theta} = r^2 \left\{ 1 + 0 \cdot \left(\frac{m}{r} \right) + 0 \cdot \left(\frac{m^2}{r^2} \right) + \mathcal{O} \left(\frac{m^3}{r^3} \right) \right\}, \quad (3.15)$$

$$g_{tt} = -1 + \frac{2m}{r} + 0 \cdot \left(\frac{m^2}{r^2} \right) + \mathcal{O} \left(\frac{m^3}{r^3} \right). \quad (3.16)$$

With (3.8)~(3.11), asymptotic forms of the metric and the scalar field near the

spatial infinity are, respectively, given by

$$\begin{aligned}
 ds^2 = & - \left[1 - \frac{2m}{r} + \left\{ \frac{1}{3} \left(\frac{\Delta^2}{\delta^2} - 1 \right) + \frac{2}{3} \left(\frac{\Delta^2 - 1}{\delta^2} \right) \left(\frac{3}{2} \cos^2 \theta - \frac{1}{2} \right) \right\} \frac{m^3}{r^3} \right] dt^2 \\
 & + \left[1 - \frac{2m}{r} + \left(\frac{\Delta^2}{\delta^2} - 1 \right) \frac{m^2}{r^2} \right]^{-1} dr^2 + r^2 (d\theta^2 + \sin^2 \theta d\phi^2),
 \end{aligned} \tag{3.17}$$

and

$$\begin{aligned}
 \frac{\delta}{d} (\varphi - \varphi_0) = & - \frac{m}{r} - \frac{m^2}{r^2} \\
 & - \left\{ \frac{3}{2} - \frac{1}{6} \left(\frac{\Delta}{\delta} \right)^2 - \left(\frac{\Delta^2 - 1}{3\delta^2} \right) \left(\frac{3}{2} \cos^2 \theta - \frac{1}{2} \right) \right\} \frac{m^3}{r^3}.
 \end{aligned} \tag{3.18}$$

Since $(d/\delta)^2 = \Delta^2/\delta^2 - 1$, these asymptotic forms include the parameters, Δ and δ , in the forms, $\Delta^2/\delta^2 - 1$ and $(\Delta^2 - 1)/\delta^2$, which can be interpreted as a squared effective amplitude of the scalar field and a non-sphericity of the spacetime symmetry, respectively. It is noted that the non-sphericity appearing in g_{tt} can be read as a quadrupole moment of the gravitational potential in Newton's theory.

3.3. Directional properties of the spacetime singularity

The scalar-tensor-Weyl solution has a coordinate singularity at $x = 1$, and it is generally a naked spacetime singularity whose qualitative features are similar to those of Voorhees's prolate solution. A spatial topology of the singularity at $x = 1$ is a sphere for $\Delta^2 \neq 1$ and becomes a point for $\Delta^2 = 1$. When $\Delta^2 = \delta = 1$, the coordinate singularity at $x = 1$ becomes an event horizon, $r = 2m$, and a true spacetime singularity at $r = 0$ is hidden by the event horizon. When $\Delta^2 \neq 1$, two poles, namely $y = 1$ and $y = -1$, on the singular surface at $x = 1$ have directional properties as shown below.

In the scalar-tensor-Weyl solution, a scalar polynomial of the curvature tensor can be calculated as

$$\begin{aligned}
 R^{\mu\nu\rho\sigma} R_{\mu\nu\sigma\rho} = & \frac{4}{\sigma^4} (x-1)^{2(\delta-\Delta^2-1)} (x+1)^{-2(\delta+\Delta^2+1)} (x^2-y^2)^{2\Delta^2-3} \times \\
 & [-4\Delta^4\delta^2(1-y^2) + 4\Delta^4\delta x(1-y^2) - 3\Delta^4(x^2-y^2) \\
 & + 8\Delta^2\delta^3x(1-y^2) - 2\Delta^2\delta^2(-4+3y^2-6y^2x^2+7x^2) \\
 & - 4\Delta^2\delta x(1+y^2-2x^2) - 7\delta^4(x^2-y^2) \\
 & - 8\delta^3x(1+y^2-2x^2) - 4\delta^2(1-y^2-3x^2+3x^4)].
 \end{aligned} \tag{3.19}$$

As a simple example, we consider a path on the (x, y) -plane given by $y = x - (x-1)^\alpha$, where α is a constant such that $0 < \alpha < 1$. This condition on the index, α , ensures that inequalities, $x > 1$ and $y < 1$, are satisfied along the path. Then one finds that the polynomial (3.19) along the path is expressed as the product of some

regular function of (x, y) and the following factor,

$$\begin{aligned} (x-1)^{2(\delta-\Delta^2-1)}(x-y)^{2\Delta^2-3} &= (x-1)^K, \\ K &\equiv (2\Delta^2-3)\alpha - 2(\Delta^2-\delta+1). \end{aligned} \quad (3\cdot 20)$$

While one finds that the polynomial (3.19) diverges along the path when $K < 0$, one does not meet any spacetime singularity along the path when $K \geq 0$. One notes that the inequality, $\Delta^2 - \delta + 1 > 0$, always holds because of the definition of Δ : $\Delta \equiv \sqrt{\delta^2 + d^2} \geq |\delta|$. The sign of the index, K , therefore depends on the sign of the coefficient, $2\Delta^2 - 3$, as follows:

(a) The case of $2\Delta^2 - 3 \leq 0$

The index, K , always becomes negative for any positive value of α , accordingly the pole, $(x, y) = (1, 1)$, is a spacetime singularity.

(b) The case of $2\Delta^2 - 3 > 0$

When $\alpha \geq \alpha_0 \equiv 1 - (2\delta - 5) / (2\Delta^2 - 3) > 0$, $K \geq 0$ holds, and one does not meet a spacetime singularity at the pole, $(x, y) = (1, 1)$, along the path.

We now summarize the conditions on the parameters, Δ and δ , such that the index, K , can be positive. When the inequality, $\delta < 2/5$, holds, the parameter, α_0 , defined for the above case (b) always becomes greater than unity. Since $0 < \alpha < 1$, two conditions, $\Delta^2 > 3/2$ and $\delta \geq 5/2$, must hold in order for K to be positive. From the another point of view, one can think of α_0 as a function of Δ and δ . Under the above conditions, $\Delta^2 > 3/2$ and $\delta \geq 5/2$, α_0 is a monotonic function of Δ and δ and has a minimal value as $\alpha_0 = (1 + \sqrt{19})/6$ for $\Delta = \delta = (5 + \sqrt{19})/2$. Consequently, the index, K , is always negative for any values of Δ and δ in the case of $0 < \alpha < (1 + \sqrt{19})/6$.

§4. Analytic results on null geodesics and optical scalars

We study the properties of irrotational null geodesics and optical scalars in the scalar-tensor-Weyl solution by analytic approaches. Hereafter, we consider the parameter, δ , to be non-negative such that $m \equiv \delta\sigma \geq 0$ holds. Accordingly, we have $0 \leq \delta \leq \Delta$ in scalar-tensor theories of gravity and $0 \leq \delta = \Delta$ in general relativity.

4.1. Null geodesics

Because of the conformally invariant nature of null geodesics, we consider null geodesics on the spacetime with the metric, $g_{\mu\nu} \equiv A^{-2}\hat{g}_{\mu\nu}$. Hereafter, a hat denotes geometrical quantities associated with $\hat{g}_{\mu\nu}$, and the corresponding geometrical quantities associated with $g_{\mu\nu}$ are denoted without a hat. Let $\hat{k}^\mu = dx^\mu/dv$ be a null geodesic tangent associated with $\hat{g}_{\mu\nu}$, where v is the affine parameter. Then a null

geodesic tangent, $k^\mu = dx^\mu/d\lambda$, associated with $g_{\mu\nu}$ is given by

$$d\lambda = A^{-2}dv, \quad k^\mu = \frac{dx^\mu}{d\lambda} = A^2\hat{k}^\mu. \quad (4.1)$$

The null vectors, \hat{k}^μ and k^μ , satisfy the following geodesic equations,

$$\hat{k}^\alpha \hat{\nabla}_\alpha \hat{k}^\mu = k^\alpha \nabla_\alpha k^\mu = 0. \quad (4.2)$$

Since it is difficult to study generic null geodesics analytically, we consider specific null geodesics which are always on the equatorial plane, $y = 0$. In this case, the geodesic equations are reduced to

$$\begin{aligned} \dot{W}^2 &= 1 - \frac{h^2}{\sigma^2(x^2 - 1)} \left(\frac{x-1}{x+1} \right)^{2\delta} \equiv 1 - V(x), \\ \dot{t} &= \left(\frac{x+1}{x-1} \right)^\delta, \quad \dot{\phi} = \frac{h}{\sigma^2(x^2 - 1)} \left(\frac{x-1}{x+1} \right)^\delta, \end{aligned} \quad (4.3)$$

where a dot denotes a differentiation with respect to the affine parameter, λ , a constant, h , is an impact parameter and W is a function of x defined by

$$\frac{dx}{dW} = \frac{1}{\sigma} \left(\frac{x^2}{x^2 - 1} \right)^{\frac{\Delta^2 - 1}{2}}. \quad (4.4)$$

One of the particular orbits of interest is a circular orbit,⁷⁾ and it is determined by the conditions that $\dot{W} = 0$ and $dV/dx = 0$. These conditions are reduced to $x = 2\delta$ when $\delta > 1/2$, and the circular orbit cannot exist when $\delta \leq 1/2$. As will be shown later, $\delta = 1/2$ is a critical value such that many geometrical quantities for $\delta < 1/2$ show very different properties compared with those for $\delta > 1/2$.

In the asymptotic region such that $r \gg m$ (see Section 3.2), the geodesic equation can be approximated by

$$\left(\frac{dr}{d\lambda} \right)^2 = 1 - \frac{h^2}{r^2} \left(1 - \frac{2m}{r} \right) + \left(1 - \frac{h^2}{r^2} \right) \left(\frac{\Delta^2}{\delta^2} - 1 \right) \frac{m^2}{r^2} + O\left(\frac{m^3}{r^3} \right), \quad (4.5)$$

which is compared with the following exact result in the Schwarzschild spacetime,

$$\left(\frac{dr}{d\lambda} \right)^2 = 1 - \frac{h^2}{r^2} \left(1 - \frac{2m}{r} \right). \quad (4.6)$$

With the reduced null geodesics equation (4.3), a deflection angle, α , of the light path is obtained as

$$\alpha(x_o) = 2 \int_{x_o}^{\infty} \frac{\left(\frac{x^2}{x^2 - 1} \right)^{\frac{1-\Delta^2}{2}}}{\sqrt{x^2 - 1} \sqrt{\frac{x^2 - 1}{x_o^2 - 1} \left(\frac{x+1}{x-1} \right)^{2\delta} \left(\frac{x_o+1}{x_o-1} \right)^{-2\delta} - 1}} dx - \pi, \quad (4.7)$$

where a parameter, x_o , is related to the impact parameter, h , by

$$h = \sigma \sqrt{x_o^2 - 1} \left(\frac{x_o + 1}{x_o - 1} \right)^\delta. \quad (4.8)$$

Since a deflection angle can be defined only for the scattering orbit, the allowed range of x_o is given by $x_o > 2\delta$ for $\delta > 1/2$ and $x_o > 1$ for $\delta \leq 1/2$, accordingly the possible range of the impact parameter is given by

$$h > h_* = \begin{cases} 2m \sqrt{1 - \frac{1}{4\delta^2}} \left(\frac{2\delta + 1}{2\delta - 1} \right)^\delta & (\delta > 1/2) \\ 4m & (\delta = 1/2) \\ 0 & (\delta < 1/2), \end{cases} \quad m = \delta\sigma \geq 0. \quad (4.9)$$

Specific values of $h_*/2m$ are, for example, 2.161, 2.543, 2.598, 2.667 and 2.690 for $\delta = 0.53, 0.7, 1.0, 1.5$ and 2.0 , respectively. The coordinate, x , decreases to the ‘‘perihelion’’, $x = x_o$, and then increases along the scattering orbit.

We obtain an analytic form of the deflection angle, $\alpha(x_o)$, in the following specific cases.

(a) $\delta = 0, \Delta^2 = 2N$ ($N = 1, 2, 3, \dots$)

$$\begin{aligned} \alpha(x_o) &= \pi \left\{ \sqrt{1 - \frac{1}{x_o^2}} \sum_{p=0}^{N-1} \frac{(-1)^p (2p-1)!! (N-1)!}{2^p (N-p-1)! (p!)^2 x_o^{2p}} - 1 \right\} \\ &= \pi \left\{ \sqrt{1 - \frac{1}{x_o^2}} \left(1 - \frac{N-1}{2x_o^2} + \frac{3(N-1)(N-2)}{16x_o^4} - \dots \right) - 1 \right\} \\ &\sim \begin{cases} -\pi & (x_o \sim 1) \\ -\frac{\pi\Delta^2}{4x_o^2} & (x_o \gg 1). \end{cases} \end{aligned} \quad (4.10)$$

One notes that it is the case of $m = 0$. The deflection angle is a negative, monotonously increasing function of x_o for any value of N , as is depicted in Figure 2a. In addition, the deflection angle can be regarded as a monotonously decreasing function of N .

(b) $\delta = 1/2, \Delta^2 = 4L + 2$ ($L = 0, 1, 2, \dots$)

(i) $L = 0$

$$\begin{aligned} \alpha(x_o) &= \pi \left\{ \frac{x_o + 1}{\sqrt{x_o(x_o + 2)}} \left[\frac{2}{\pi} \sin^{-1} \frac{1}{x_o + 1} + 1 \right] - 1 \right\} \\ &\sim \begin{cases} \pi \left(\frac{8\sqrt{3}}{9} - 1 \right) > 0 & (x_o \sim 1) \\ \frac{2}{x_o} - \left(2 - \frac{\pi}{2} \right) \frac{1}{x_o^2} & (x_o \gg 1). \end{cases} \end{aligned} \quad (4.11)$$

(ii) $L \geq 1$

$$\begin{aligned}
 \alpha(x_o) &= 2\sqrt{x_o(x_o+2)} \left[\frac{x_o+1}{x_o(x_o+2)} \right]^{4L+1} I_L(x_o) - \pi, \\
 I_L(x_o) &= \sum_{n=0}^L \sum_{k=0}^{2n} \frac{(2L)!}{(2L-2n)!(2n-k)!k!} \eta(x_o)^{2(L-n)} \xi(x_o)^k A_\ell(x_o) \\
 &\quad + \sum_{n=0}^{L-1} \sum_{k=0}^{2n+1} \frac{(2L)!}{(2L-2n-1)!(2n-k+1)!k!} \eta(x_o)^{2(L-n)-1} \xi(x_o)^k B_\ell(x_o), \\
 A_p(x_o) &= \frac{(2p-1)!!}{(2p)!!} \left\{ \frac{\pi}{2} + \sin^{-1} \frac{1}{x_o+1} \right. \\
 &\quad \left. - \frac{\sqrt{x_o(x_o+2)}}{x_o+1} \sum_{r=0}^{p-1} \frac{(2p-2r-2)!!}{(2p-2r-1)!!} \frac{1}{(x_o+1)^{2p-2r-1}} \right\}, \\
 B_p(x_o) &= \frac{(2p)!!}{(2p+1)!!} \frac{\sqrt{x_o(x_o+2)}}{x_o+1} \sum_{r=0}^p \frac{(2p-2r-1)!!}{(2p-2r)!!} \frac{1}{(x_o+1)^{2p-2r}},
 \end{aligned} \tag{4.12}$$

where $\eta(x_o) = 2/(x_o+1)$, $\xi(x_o) = 1 - 2x_o - x_o^2$ and $\ell = L + n - k$.

(c) $\delta = 1/2$, $\Delta^2 = 4L + 4$ ($L = 0, 1, 2, \dots$)

$$\begin{aligned}
 \alpha(x_o) &= -2\sqrt{x_o(x_o+2)} \left[\frac{x_o+1}{x_o(x_o+2)} \right]^{4L+3} J_L(x_o) - \pi, \\
 J_L(x_o) &= \sum_{n=0}^L \sum_{k=0}^{2n+1} \frac{(2L+1)!}{(2L-2n)!(2n-k+1)!k!} \eta(x_o)^{2(L-n)} \xi(x_o)^k A_{\ell+1}(x_o) \\
 &\quad + \sum_{n=0}^L \sum_{k=0}^{2n} \frac{(2L+1)!}{(2L-2n+1)!(2n-k)!k!} \eta(x_o)^{2(L-n)+1} \xi(x_o)^k B_\ell(x_o),
 \end{aligned} \tag{4.13}$$

where $\ell = L + n - k$. The functions, $\eta(x_o)$, $\xi(x_o)$, $A_p(x_o)$ and $B_p(x_o)$, are the same as those of the case (b).

The above two cases, (b) and (c), are grouped into the single case that $\delta = 1/2$ and $\Delta^2 = 2N$, where N is a positive integer. We depict the deflection angle for several values of N in Figure 2b. It should be noted that, unless N is unity, the deflection angle for small values of the impact parameter, h , can become a negative, increasing function of h in marked contrast with the case of the Schwarzschild spacetime.

The appearance of a negative deflection angle indicates ‘‘reflection’’ of a light path, and we will later study under which conditions the light reflection occurs.

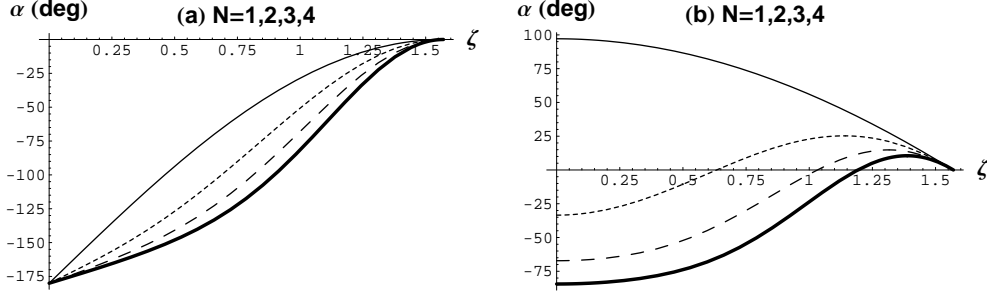


Fig. 2. The deflection angle, $\alpha(x_o)$, is shown for some specific values of the parameters, (δ, Δ) , where ζ is defined by $x_o = 1/\cos \zeta$, and $\alpha(x_o)$ is given in the unit of degree. The model parameters are (a) $\delta = 0$, $\Delta^2 = 2N$ and (b) $\delta = 1/2$, $\Delta^2 = 2N$. We use a thin line for $N = 1$, a short broken line for $N = 2$, a long broken line for $N = 3$ and a bold line for $N = 4$.

4.2. Optical scalars

Since the local geometrical nature of the spacetime is described by the Riemann curvature, it is important to investigate the properties of optical scalars of the irrotational null geodesic congruence.¹⁰⁾ Let $\{\hat{\mathbf{E}}_{(1)}, \hat{\mathbf{E}}_{(2)}, \hat{\mathbf{E}}_{(3)}, \hat{\mathbf{E}}_{(4)}\} = \{\hat{\mathbf{k}}, \hat{\mathbf{m}}, \hat{\mathbf{t}}, \hat{\bar{\mathbf{t}}}\}$ be a null tetrad such that

$$\hat{k}^\mu \hat{\nabla}_\mu \hat{E}_{(a)}^\nu = 0, \quad \hat{g}_{\mu\nu} \hat{E}_{(a)}^\mu \hat{E}_{(b)}^\nu = -\delta_a^1 \delta_b^2 - \delta_a^2 \delta_b^1 + \delta_a^3 \delta_b^4 + \delta_a^4 \delta_b^3. \quad (4.14)$$

Then the optical scalars, namely, the expansion, θ , and the complex shear, σ , are defined by

$$\hat{\theta} = \hat{\nabla}_\mu \hat{k}_\nu \hat{t}^\mu \hat{\bar{t}}^\nu, \quad \hat{\sigma} = \hat{\nabla}_\mu \hat{k}_\nu \hat{t}^\mu \hat{t}^\nu. \quad (4.15)$$

The optical scalar equations are also conformally invariant, and we define the following quantities associated with $g_{\mu\nu}$,⁷⁾

$$\theta = A^2 \hat{\theta} - k^\mu \nabla_\mu \ln A, \quad \sigma = A^2 \hat{\sigma}, \quad t^\mu = A \hat{t}^\mu, \quad \bar{t}^\mu = A \hat{\bar{t}}^\mu. \quad (4.16)$$

Then the optical scalar equations become^{10), 11)}

$$\frac{d\theta}{d\lambda} + \theta^2 + |\sigma|^2 = -\frac{1}{2} R_{\mu\nu} k^\mu k^\nu \equiv -\mathcal{R}, \quad (4.17)$$

$$\frac{d\sigma}{d\lambda} + 2\theta\sigma = -R_{\mu\alpha\nu\beta} k^\mu k^\nu \bar{t}^\alpha \bar{t}^\beta = -C_{\mu\alpha\nu\beta} k^\mu k^\nu \bar{t}^\alpha \bar{t}^\beta \equiv F, \quad (4.18)$$

where $C_{\mu\alpha\nu\beta}$ is the Weyl curvature.

Dyer has obtained general solutions to the optical scalar equations in the general static, spherically symmetric spacetime.¹¹⁾ We summarize his results in Appendix C, and one finds that the Weyl source-term, F , and the shear, σ , can be regarded as real quantities without loss of generality.¹¹⁾ Though the scalar-tensor-Weyl solution is not spherically symmetric, we can apply Dyer's method as concerns the null geodesics

on the equatorial plane, $y = 0$.⁷⁾ By defining the new optical scalars, C_+ and C_- , as

$$\frac{d}{d\lambda} \ln C_+ = \theta + \sigma, \quad \frac{d}{d\lambda} \ln C_- = \theta - \sigma, \quad (4.19)$$

Dyer has obtained the following equations,

$$\frac{d^2 C_+}{d\lambda^2} = (-\mathcal{R} + F)C_+, \quad \frac{d^2 C_-}{d\lambda^2} = (-\mathcal{R} - F)C_-. \quad (4.20)$$

The equations (4.20) are equivalent to the geodesic deviation equations, and the variables, C_+ and C_- , represent, respectively, the size of the major axis and the minor axis of the infinitesimal image in the Einstein frame. We define the conformal transformation of C_{\pm} by $\hat{C}_{\pm} = AC_{\pm}$ such that this transformation law is compatible with the others.

The Ricci and Weyl source-terms, $\mathcal{R}(x)$ and $F(x)$, in the Scalar-tensor-Weyl solution on the equatorial plane, $y = 0$, are calculated as (Appendix C, Ref.7)

$$\begin{aligned} \mathcal{R}(x) &= \frac{\Delta^2 - \delta^2}{\sigma^2} \frac{1}{x^2(x^2 - 1)} \left(\frac{x^2}{x^2 - 1} \right)^{\Delta^2} \left[1 - \frac{(h/\sigma)^2}{x^2 - 1} \left(\frac{x - 1}{x + 1} \right)^{2\delta} \right] \\ &= \frac{\Delta^2 - \delta^2}{(x^2 - 1)^2} (k^1)^2, \quad k^1 = \frac{dx}{d\lambda}, \end{aligned} \quad (4.21)$$

$$\begin{aligned} F(x) &= \frac{1}{\sigma^2} \frac{1}{x^3(x^2 - 1)} \left(\frac{x^2}{x^2 - 1} \right)^{\Delta^2} \times \tilde{F}(x), \\ \tilde{F}(x) &= \delta(\Delta^2 - 1) \\ &\quad + \frac{(h/\sigma)^2}{x^2 - 1} \left(\frac{x - 1}{x + 1} \right)^{2\delta} \{ \delta(\Delta^2 - 1) - (\Delta^2 + 2\delta^2)x + 3\delta x^2 \}, \end{aligned} \quad (4.22)$$

where h is the impact parameter as before. In general relativity, we have $\Delta = \delta$ and $\mathcal{R}(x) = 0$. In the asymptotic region such that $x \gg 1$, $\mathcal{R}(x)$ and $F(x)$, respectively, approximate to

$$\mathcal{R}(x) \sim \frac{m^2 (\Delta^2 - \delta^2)}{\delta^2 r^4} \left[1 + \frac{4m}{r} - \frac{h^2}{r^2} \left(1 + \frac{m}{r} \right) \right], \quad (4.23)$$

$$F(x) \sim \frac{3mh^2}{r^5} \left(1 - \frac{\Delta^2 - \delta^2}{3\delta^2} \frac{m}{r} + \frac{4\Delta^2 + \delta^2 - 5m^2}{6\delta^2} \frac{m^2}{r^2} \right) + \frac{\Delta^2 - 1}{\delta^2} \frac{m^3}{r^5}, \quad (4.24)$$

in terms of m/r , where x is related to r by (3.8)~(3.11) with $y = 0$.

It is immediately found that the Ricci source-term, $\mathcal{R}(x)$, satisfies $\mathcal{R}(x) \geq 0$ and necessarily vanishes at the perihelion, $x = x_o$, because k^1 vanishes there. As for the Weyl source-term, $F(x)$, its value is not always positive and can become negative along the light path. Since the Weyl source-term is mostly dominant over the Ricci source-term as will be found by the later numerical study, we classify the parameter space, (δ, Δ) , according to the qualitative properties of the Weyl source-term as follows.

When $\delta = \Delta = 1$, the scalar-tensor-Weyl solution becomes the Schwarzschild spacetime, and we have

$$F(x) = \frac{3h^2}{\sigma^4(x+1)^5} = \frac{3mh^2}{r^5}. \quad (4.25)$$

One notes that the Weyl source-term (4.25) has the following properties:

- A1** It is strictly positive definite for $x > x_o$.
- A2** It is a monotonously decreasing function of x .
- A3** It takes the maximum value at the perihelion, $x = x_o$, along the scattering orbit.

Because of the properties above, one may simply expect that light rays are affected by the Weyl source-term mostly near the perihelion. For this reason, we first classify the parameter space, (δ, Δ) , according to the value of $F(x_o)$. With (4.8) and (4.22), one finds that

$$\begin{aligned} F(x_o) &= \frac{1}{\sigma^2} \frac{1}{x_o^3(x_o^2-1)} \left(\frac{x_o^2}{x_o^2-1} \right)^{\Delta^2} f(x_o), \\ f(x_o) &= 3\delta x_o^2 - (\Delta^2 + 2\delta)x_o + 2\delta(\Delta^2 - 1). \end{aligned} \quad (4.26)$$

The most intriguing thing is that $F(x_o)$ becomes zero for $x_o = x_{F+}$ and $x_o = x_{F-}$, where

$$\begin{aligned} x_{F\pm} &= \frac{1}{6\delta} \left\{ (\Delta^2 + 2\delta^2) \pm \sqrt{D} \right\}, \\ D &= (\Delta^2 - 10\delta^2)^2 - 24\delta^2(2\delta - 1)(2\delta + 1). \end{aligned} \quad (4.27)$$

Note that $x_{F\pm}$ and D are, respectively, roots and a discriminant of the quadratic equation, $f(x_o) = 0$. Since x_o should be real and moreover satisfy the condition, $x_o > 2\delta$ for $\delta > 1/2$ and $x_o > 1$ for $\delta \leq 1/2$, we classify the parameter space, (δ, Δ) , on the basis of the number of the conditional roots as follows:

(a) The region of $\delta > 1/2$

The discriminant, D , should be positive or zero in order for $x_{F\pm}$ to be real, and this condition is satisfied for the two cases, namely the case of $\Delta^2 \leq \Delta_-^2$ and the case of $\Delta^2 \geq \Delta_+^2$, where

$$\Delta_{\pm}^2 = 10\delta^2 \pm \sqrt{24\delta^2(2\delta - 1)(2\delta + 1)}. \quad (4.28)$$

For $\delta > 1/2$, Δ_+^2 and Δ_-^2 are always real and moreover satisfy the relation, $0 < \Delta_-^2 < \Delta_+^2$. In this region, a further condition, $x_o > 2\delta$, should be satisfied for the scattering orbit, and we find that it holds only for the case, $\Delta^2 \geq \Delta_+^2$, and is always violated for the case, $\Delta^2 \leq \Delta_-^2$. We also find that the case of $x_{F-} < 2\delta < x_{F+}$ does not occur. The equations, $\Delta = \Delta_+$ and $\delta = 1/2$, define the

critical lines on the parameter space, (δ, Δ) , on which $x_{F+} = x_{F-}$ and $\Delta_+^2 = \Delta_-^2$ hold, respectively. In summary, the region of $\delta > 1/2$ is classified into the following two regions:

(i) $\Delta^2 < \Delta_+^2$

We shall refer to the region determined by the conditions, $\delta > 1/2$ and $\Delta^2 < \Delta_+^2$, as the region N_A (N: none) because the equation, $F(x_o) = 0$, has no conditional root in this region.

(ii) $\Delta^2 > \Delta_+^2$

We shall refer to the region determined by the conditions, $\delta > 1/2$ and $\Delta^2 > \Delta_+^2$, as the region II (II: two) because the equation, $F(x_o) = 0$, has two conditional roots, x_{F+} and x_{F-} , in this region.

(b) The region of $0 < \delta < 1/2$

The quadratic equation, $f(x_o) = 0$, always has two real roots, x_{F+} and x_{F-} , because its discriminant, D , is positive-definite for $0 < \delta < 1/2$. In this region, a further condition, $x_o > 1$, should be satisfied for the scattering orbit, and we find that x_{F-} is inevitably less than unity. The condition, $x_{F+} > 1$, can be reduced to $\delta < \Delta^2$, and we have $x_{F+} = 1$ on the new critical line defined by $\delta = \Delta^2$. In summary, the region of $0 < \delta < 1/2$ is classified into the following two regions:

(i) $\delta < \Delta^2$

We shall refer to the region determined by the conditions, $0 < \delta < 1/2$ and $\delta < \Delta^2$, as the region I (I: one) because the equation, $F(x_o) = 0$, has a single conditional root, x_{F+} , in this region.

(ii) $\delta > \Delta^2$

We shall refer to the region determined by the conditions, $0 < \delta < 1/2$ and $\delta > \Delta^2$, as the region N_B because the equation, $F(x_o) = 0$, has no conditional root in this region.

(c) The critical line, $\delta = 1/2$

We have a single conditional root, $x_{F+} = 2(\Delta^2 - 1)/3$, for $\Delta^2 > 5/2$ and no root for $\Delta^2 \leq 5/2$.

(d) $\delta = 0$

For any positive value of Δ^2 , $F(x_o)$ is negative.

The results of the above classification are shown in Figure 3.

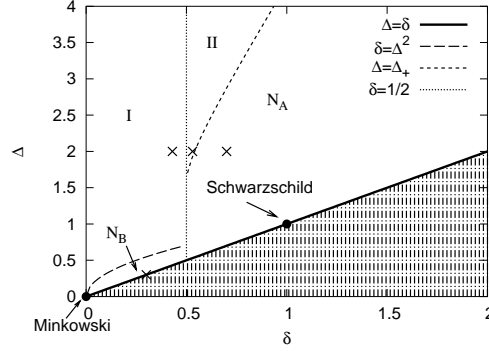


Fig. 3. We classify the parameter space, (δ, Δ) , into four regions (N_A , N_B , I and II) according to the number of roots of a quadratic equation, $f(x_o) = 0$, with the additional conditions described in the text. Horizontal and vertical axes denote δ and Δ , respectively, and $\Delta \geq \delta$ in the scalar-tensor-Weyl solution. Three critical lines, $\delta = 1/2$, $\delta = \Delta^2$ and $\Delta = \Delta_+$, are shown, where Δ_+ is given by $\Delta_+^2 = 10\delta^2 + \delta\sqrt{24(2\delta - 1)(2\delta + 1)}$. Two specific points, $(\delta, \Delta) = (0, 0)$ and $(\delta, \Delta) = (1, 1)$, represent the Minkowski spacetime and the Schwarzschild spacetime, respectively. When we show some typical examples of the numerical results, we will mostly consider the points denoted by \times as standard ones (see Section 5.1).

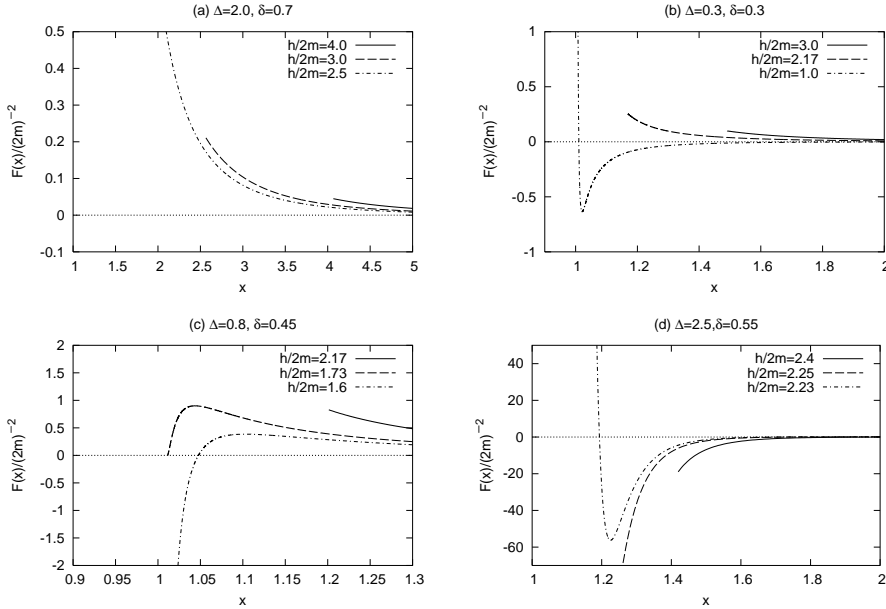


Fig. 4. The Weyl source-term, $F(x)$, is shown as a function of x ($x_o < x$) for several values of Δ and δ : (a) $(\delta, \Delta) = (0.7, 2.0)$ in the region N_A , (b) $(\delta, \Delta) = (0.3, 0.3)$ in the region N_B , (c) $(\delta, \Delta) = (0.45, 0.8)$ in the region I and (d) $(\delta, \Delta) = (0.55, 2.5)$ in the region II.

In Figure 4, we show the Weyl source-term, $F(x)$, as a function of x ($x_o < x$) for several values of the parameters, δ and Δ , and the impact parameter, h . While $F(x)$ has similar properties as those in the case of the Schwarzschild spacetime for large h (see A1~A3), the following quite different properties B1~B3 can appear for small h .

B1 It can be negative, and the maximum number of roots of the equation, $F(x) = 0$, is two for $x > x_o$.

B2 It can have extremes, and the maximum number of the extremes is two for $x > x_o$.

B3 It does not necessarily take the maximum value at the perihelion, $x = x_o$, along the scattering orbit.

We numerically investigate the function, $F(x)$, and classify the parameter space, (δ, Δ) , by the maximum number of the roots (B1) and the maximum number of the extremes (B2). The results are summarized in Figure 5. In Figure 5a, the maximum number of the roots is shown by symbols, * and +. In the region denoted by *, there exists at least one impact parameter, h , such that $F(x) = 0$ has two roots. In the region denoted by +, $F(x) = 0$ cannot have two roots for any h , and there exists at least one impact parameter, h , such that $F(x) = 0$ has a single root. In the blank region, $F(x) = 0$ cannot have a root for any h . The maximum number of the extremes is shown in Figure 5b in the similar manner as in the case of Figure 5a, namely * for two extremes, + for one extreme at the maximum and blank for no extreme. One immediately finds close resemblance between these classified regions in Figures 5a,b and the previous one in Figure 3. We will numerically show that the classification presented in Figure 3 really has a close relationship with several properties of light propagation and gravitational lensing.

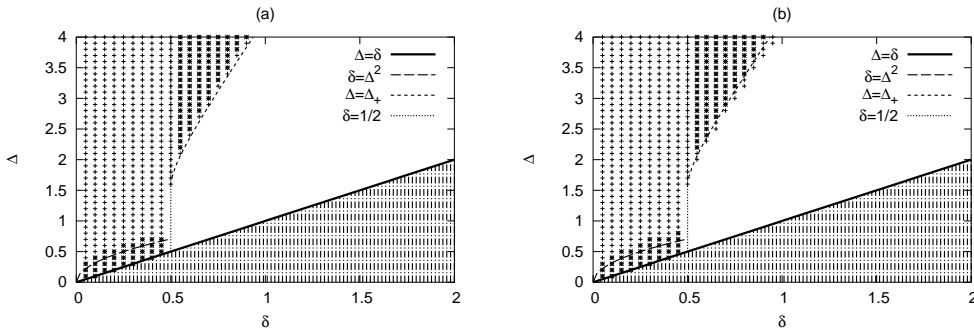


Fig. 5. We classify the parameter space, (δ, Δ) , according to the qualitative properties of the Weyl source-term, $F(x)$: (a) classification by the maximum number of roots of $F(x) = 0$ and (b) classification by the maximum number of extremes of $F(x)$. Further details of these figures are explained in the text.

§5. Numerical results on null geodesics and optical scalars

Now we will show several numerical results on null geodesics and optical scalars.

5.1. Preliminaries

There are three model parameters, σ , δ and Δ , in the scalar-tensor-Weyl solution, and we reduce the number of the parameters to two by fixing the values of $m \equiv \delta\sigma$. In other words, m plays the role of a unit of length. When we show some typical examples of the numerical results, the following values of the model parameters, (δ, Δ) , will mostly be considered as standard ones (see Figure 3),

$$(\delta, \Delta) = \begin{cases} [\text{n}_A] & (0.7, 2.0) & \text{in the region } N_A \\ [\text{n}_B] & (0.3, 0.3) & \text{in the region } N_B \\ [\text{i}] & (0.43, 2.0) & \text{in the region I} \\ [\text{ii}] & (0.53, 2.0) & \text{in the region II} . \end{cases} \quad (5.1)$$

In Section 4.2 we have investigated the conditional roots of the equation, $F(x_o) = 0$, and find the single root, x_{F+} , in the regions I and the two roots, x_{F+} and x_{F-} in the region II. These roots, x_{F+} and x_{F-} , are related to the impact parameters, h_{F+} and h_{F-} , by

$$\begin{aligned} h_{F+} &= \sigma \sqrt{x_{F+}^2 - 1} \left(\frac{x_{F+} + 1}{x_{F+} - 1} \right)^\delta, \\ h_{F-} &= \sigma \sqrt{x_{F-}^2 - 1} \left(\frac{x_{F-} + 1}{x_{F-} - 1} \right)^\delta, \end{aligned} \quad (5.2)$$

respectively. We will repeatedly emphasize the importance of these specific values of the impact parameter, h_{F+} and h_{F-} .

On the equatorial plane, $y = 0$, a spatial part of the metric (3.1) becomes

$$ds^2 = \frac{m^2}{\delta^2} \left(\frac{x-1}{x+1} \right)^{-\delta} \left[\left(\frac{x^2-1}{x^2} \right)^{\Delta^2-1} dx^2 + (x^2-1)d\phi^2 \right], \quad (5.3)$$

and the equatorial circumference, L_x , is given by

$$L_x = 2\pi R_x(x), \quad R_x(x) \equiv \frac{m}{\delta} \left(\frac{x-1}{x+1} \right)^{-\frac{\delta}{2}} \sqrt{x^2-1}. \quad (5.4)$$

On the basis of this geometrical consideration, we define the dimensionless, locally Cartesian-like coordinates, (X, Y) , by

$$X = \frac{R_x(x)}{2m} \cos \phi, \quad Y = \frac{R_x(x)}{2m} \sin \phi, \quad (5.5)$$

for the sake of later convenience.

The optical scalar equations should be solved along the corresponding light path, and therefore, we numerically integrate the geodesic equations and the optical scalar equations simultaneously under the initial conditions as follows:

- (a) The direction of the X -axis is chosen such that a light ray initially propagates in the opposite direction to the X -axis, namely from “right” to “left” in Figure 6.
- (b) The affine parameter, λ , is chosen such that $\lambda = 0$ at the initial time.
- (c) Let x_i be an initial value of the coordinate, x , of the null geodesic at $\lambda = 0$. We should determine x_i such that an initial circumference radius, $R_i \equiv R_x(x_i)$, is an approximately parameter-independent value. For $x_i = 100\delta$, we have

$$\begin{aligned} R_i/m &= \frac{1}{\delta} \left(\frac{x_i - 1}{x_i + 1} \right)^{-\frac{\delta}{2}} \sqrt{x_i^2 - 1} \\ &= \frac{x_i}{\delta} \left\{ 1 + \frac{\delta}{x_i} + \mathcal{O}\left(\frac{\delta^2}{x_i^2}\right) \right\} \sim 101 + \mathcal{O}(10^{-2}). \end{aligned} \quad (5.6)$$

Unless otherwise noted, we let a value of x_i be 100δ .

Along the scattering orbit, x decreases from x_i to its minimum values, x_o , and then increases to x_i . When x becomes x_i again at $\lambda = \lambda_f$, numerical integrations are terminated. We shall call $\lambda = \lambda_f$ the final time. Under this geometrical configuration, we define the Einstein radius, h_E , by

$$\frac{h_E}{2m} \equiv \sqrt{\frac{R_i}{2m}} \sim 7. \quad (5.7)$$

The Einstein radius, h_E , is usually defined in the weak gravity region such that $m/h_E \ll 1$, and the above estimate of h_E is compatible with the assumption that the gravity is comparatively weak even at the Einstein radius.

- (d) As for the optical scalars, their initial conditions at $\lambda = 0$ are chosen as

$$C_+ = C_- = 0, \quad \frac{dC_+}{d\lambda} = \frac{dC_-}{d\lambda} = 1, \quad (5.8)$$

such that we have $C_+ = C_- = \lambda$ in the Minkowski spacetime.

Now we should remind ourselves that the optical scalars are conformally variant as $\hat{C}_\pm = AC_\pm$. We shall therefore define a conformally invariant optical scalar, C , by

$$C \equiv \frac{C_+ - C_-}{C_+} = \frac{\hat{C}_+ - \hat{C}_-}{\hat{C}_+}. \quad (5.9)$$

Since \hat{C}_+ and \hat{C}_- represent the size of the major axis and the minor axis of the infinitesimal image, respectively, the new variable, C , is a measure of the image distortion rate. When either C_+ or C_- vanishes at the final time for some value of

the impact parameter, h , we shall refer to this specific value of the impact parameter as a caustic point. It is important to note that we have two kinds of caustic points, namely the caustic point associated with C_- and the one associated with C_+ . At the caustic point, we have $C \rightarrow 1$ for $C_- \rightarrow 0$ and $|C| \rightarrow \infty$ for $C_+ \rightarrow 0$.

5.2. Null geodesics and the deflection angle

We show the trajectories of light rays on the (X, Y) -plane in Figure 6. The model parameters, (δ, Δ) , are chosen to be the standard ones and the impact parameter, h , is chosen as (a) $h/2m = 3.0$ and (b) $h/2m = 2.17$, respectively. For the case (b), the light path in the case $[n_A]$ fails to be a scattering orbit, and therefore, we omit this case in Figure 6b. Figure 6c is an enlarged picture of the central part of Figure 6b. When the impact parameter, h , is comparatively large as in the case of Figure 6a, the gravity acts attractively, and the effects of the scalar field and the non-sphericity remain quantitative. In contrast to that, Figure 6c shows us that the gravity can act repulsively for smaller values of h , as has already been predicted by the existence of the negative deflection angle in the previous section.

The appearance of the repulsive trajectories explicitly proves that “reflection” of a light path can actually occurs, and we now investigate the conditions for that. By the simple geometrical consideration, one finds that the situation of

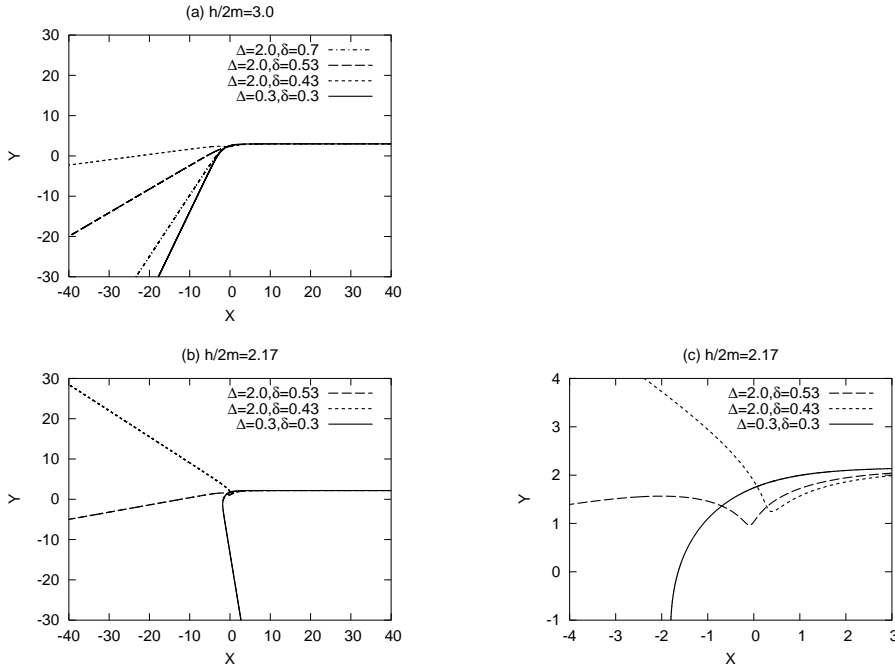


Fig. 6. The trajectories of light rays are shown on the (X, Y) -plane for (a) $h/2m = 3.0$ and (b) $h/2m = 2.17$. The enlarged central part of (b) is shown in (c).

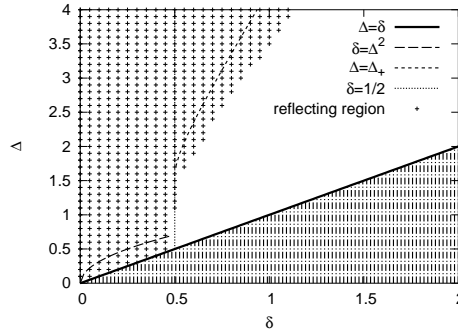


Fig. 7. The reflecting region is shown by symbols, +, on the classified parameter space, (δ, Δ) .

$d/d\lambda(dY/dX) > 0$ inevitably occurs along a reflecting, counterclockwise light path around the singularity at $x = 1$. We succeed in reducing this condition to the occurrence of $p(x) < 0$, where an auxiliary function, $p(x)$, is defined by

$$\begin{aligned}
 p(x) &= \frac{h}{\sigma^4 x^3 (x^2 - 1)^2} \left(\frac{x^2}{x^2 - 1} \right)^{\Delta^2} \times q(x), \\
 q(x) &= \{(\delta^2 - \Delta^2)x + (\Delta^2 - 1)\delta\} \left\{ h^2 \left(\frac{x-1}{x+1} \right)^{2\delta} - \sigma^2 (x^2 - 1) \right\} \\
 &\quad + h^2 x \left(\frac{x-1}{x+1} \right)^{2\delta} \left\{ x^2 \left(\frac{x^2 - 1}{x^2} \right)^{\Delta^2} - x^2 + 3\delta x - 2\delta^2 \right\}. \quad (5.10)
 \end{aligned}$$

In particular, we have $p(x) = 3mh^2/r^5 > 0$ in the Schwarzschild spacetime.

In Figure 7, we numerically compare the previously classified four regions, $N_A \sim \text{II}$, with the reflecting region in which the inequality, $p(x) < 0$, can apply. Though their relationship is halfway close, it is an intriguing thing that some parts of the boundary of the reflecting region coincide with the critical line, $\delta = 1/2$.

As for the deflection angle, we numerically integrate (4.7) with (4.8) and depict it as a function of the impact parameter, h , in Figure 8, where the marks, h_1 , h_2 and h_3 , represent the following specific values of the impact parameters, respectively:

$$(h_1, h_2) = (h_{F-}, h_{F+}) \text{ in the case [ii],} \quad h_3 = h_{F+} \text{ in the case [i].} \quad (5.11)$$

We numerically find that the deflection angle generically has two extremes near $h = h_{F+}$ and $h = h_{F-}$ in the region II and a single extreme near $h = h_{F+}$ in the region I. Graphs of the deflection angle in the regions, I and N_B , have the similar properties as follows:

C1 It has a single extreme and the extreme is the maximum.

C2 The deflection angle remains to be finite as the impact parameter approaches to zero.

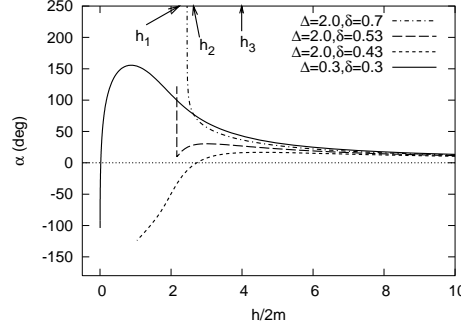


Fig. 8. The deflection angle, α , is shown as a function of the impact parameter, h . The model parameters are chosen to be the standard ones.

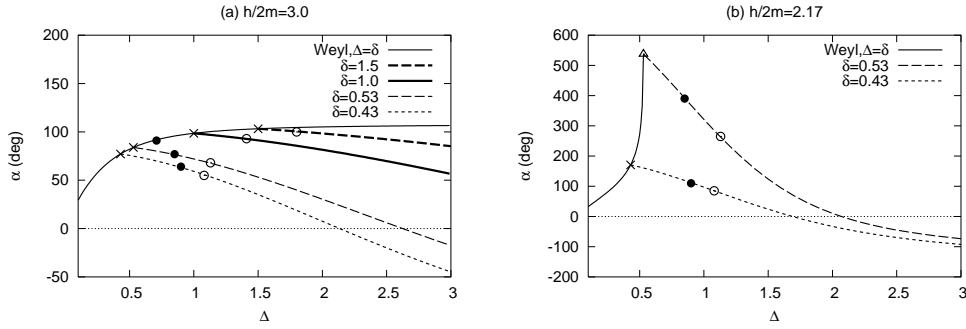


Fig. 9. The deflection angle, α , is shown as a function of the parameter, Δ , for (a) $h/2m = 3.0$ and (b) $h/2m = 2.17$. Thin lines show the deflection angles in the Weyl solution ($\Delta = \delta$). For general cases of $\Delta \geq \delta$, lines corresponding to the constant δ have terminal points (\times in the figures) on the thin line. Open circles and filled circles denote the data points such that $Q = 1$ and $Q = -1$, respectively, where $Q \equiv (\Delta^2 - 1)/\delta^2$ is a measure of the non-sphericity of the spacetime symmetry. An open triangle in (b) denotes the case that the scattering orbit cannot exist.

In particular, the properties, C1, are unexpected ones because of the absence of the characteristic scales, h_{F+} and h_{F-} , in the region N_B . Let h_α be a new characteristic value of h at which a graph of the deflection angle has the maximum. We numerical find that h_α continuously changes beyond the boundaries between the region I and the region N_B and that $h_\alpha = 2m \sim 6m$ in the region N_B . We also find that h_α is a decreasing function of δ and is an increasing function of Δ .

By fixing the values of δ and h , we show the deflection angle as a function of Δ in Figure 9 and find that the deflection angle is always a decreasing function of Δ . We also show the cases in general relativity ($\Delta = \delta$) for comparison.

By further numerical investigation on the parameter space, (δ, Δ) , we find the following notable properties of the deflection angle, $\alpha(h)$.

D1 While it is positive definite in the Schwarzschild spacetime, it can be negative

in the Scalar-tensor-Weyl solution.

D2 While it is a monotonously decreasing function of h in the Schwarzschild spacetime, it can have two extremes at the maximum.

D3 Since a circular orbit exists when $\delta > 1/2$, a light ray passing by the circular orbit can wind around it many times, and the deflection angle becomes very large. In contrast to the cases of $\delta > 1/2$, it always remains to be finite in the case of $0 \leq \delta < 1/2$ even when h approaches zero. In the case of $\delta = 1/2$, we analytically find that it remains to be finite for $\Delta > 1$ and diverges for $\Delta \leq 1$ when h approaches $4m$.

We classify the parameter space, (δ, Δ) , according to the number of extremes of $\alpha(h)$ and compare this new classification with the previous one, as is shown in Figure 10. The similar classification according to the occurrence of negative deflection angles is also done, as is shown in Figure 11. One may immediately note the surprising coincidences among these results found in Figures 10 and 11. Though we have not yet succeeded in explaining the reasons for these coincidences, we expect that the classification shown in Figure 3 may have some physical significance for gravitational lensing properties. As for the light reflection and the deflection angle, we find that their properties in the region N_B is quite similar to those in the region I.

Finally, it should be noted that this kind of the light reflection can be possible even in general relativity. That is, the light reflection inevitably occurs even on the line, $\Delta = \delta$, for $\delta < 1/2$. On the other hand, the appearance of the region II must be an intrinsic effect to the scalar-tensor theories of gravity, and we expect that the II-like region may always exist not only in the scalar-tensor-Weyl solution but also in most of the other solutions. While the boundary between the N_A -like region and the I-like region will always be clear, the boundary between the N_A -like region and the II-like region may, however, be slightly vague, as has seen in Figures 7, 10 and 11.

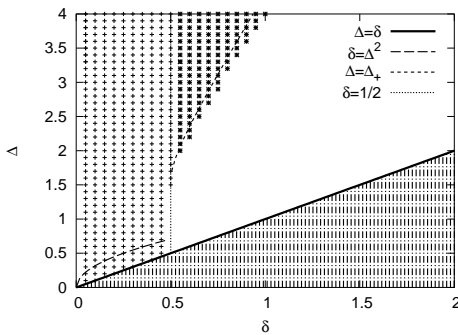


Fig. 10. We classify the parameter space, (δ, Δ) , into three regions according to the number of extremes of $\alpha(h)$: * for two extremes, + for a single extreme and *blank* for no extreme.

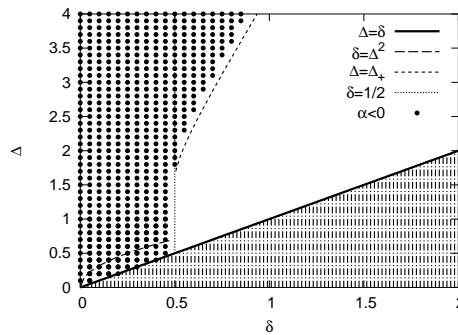


Fig. 11. We classify the parameter space, (δ, Δ) , into two regions according to the occurrence of negative deflection angles. In the region with filled circles, a deflection angle can be negative.

5.3. Optical scalars and the image distortion rate

We numerically solve the optical scalar equations along the light path by the procedure described in Section 5.1. In Figure 12, we show (a) C_+ and (b) C_- as functions of the affine parameter, λ , for several values of the impact parameters, h . The model parameters are chosen as those of the case $[n_A]$, where $(\delta, \Delta) = (0.7, 2.0)$. One must find at first sight that gravitational effects of the source-terms, F and \mathcal{R} , on the light rays appear as a rapidly changing slope of the graph of C_+ in the vicinity of $\lambda = 50$. As for C_- , the slope changes once for $h/2m = 3.0$ and 4.0 and twice for $h/2m = 2.5$. This “bending” of the graph is found in the narrow range of λ , and its width, $\Delta\lambda$, is $2 \sim 3$ for the case of C_- with $h/2m = 2.5$ and invisibly thin for the other ones. In this sense, a picture of the thin lens is applicable, and, roughly speaking, the gravitational effects appear as a bending angle of the graph.

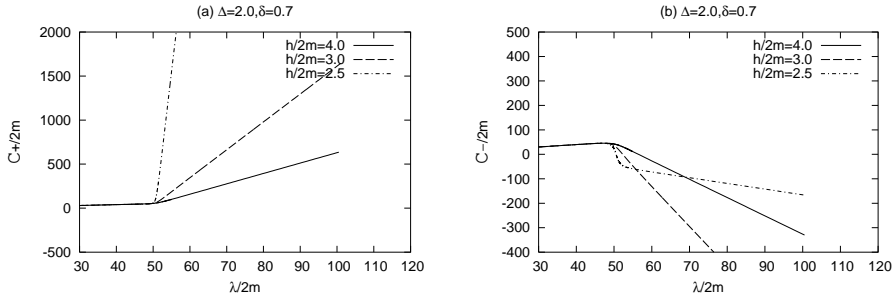


Fig. 12. We show (a) C_+ and (b) C_- as functions of λ for several values of the impact parameters, h , as denoted in each figure. The model parameters are chosen as those of the case $[n_A]$, where $(\delta, \Delta) = (0.7, 2.0)$.

In Figures 13, 14 and 15, we show (a) C_+ and (c) C_- for the standard cases, $[n_B]$, $[i]$ and $[ii]$. For comparison, the enlarged pictures of these graphs are also shown in (b) and (d) for C_+ and C_- , respectively. In any case, a rough picture of the thin lens is applicable again. To confirm the forecast that the lenses are thin, we show the Ricci and Weyl source-terms as functions of the affine parameter, λ , in Figures 16~19. These thin lenses are, however, divided into the following two groups by their thinness (or thickness).

E1 A lens is invisibly thin such that the bending angle of the graph is a moderately varying function of the impact parameter, h .

E2 A lens has a visibly finite thickness, $\Delta\lambda$, such that one recognizes a comparatively rapid variation of the graph when light rays goes through the lens.

It should be noted that the above classification of lenses is brought not so much by the intrinsic properties of each classified region in the parameter space as by the extrinsic factors, especially the impact parameter, h , and the initial distance, R_i , as

is explained by the following simple model.

Under the thin lens assumption, we approximate the optical scalar equations (4.20) by

$$\frac{d^2 u_{\pm}}{d\lambda^2} = \begin{cases} 0 & (|\lambda| > \epsilon) \\ \pm \kappa^2 u_{\pm} & (|\lambda| < \epsilon), \end{cases} \quad (5.12)$$

where κ^2 and $\epsilon \sim \Delta\lambda/2$ are an amplitude of the source-term and a thickness of the lens, respectively. The affine parameter, λ , is redefined such that the center of the thin lens is at $\lambda = 0$. For example, when the combined source-term, $-\mathcal{R} + F$, of C_+ is negative, the negative sign of (5.12) is chosen for C_+ :

$$\frac{d^2 C_+}{d\lambda^2} = (-\mathcal{R} + F) C_+ \rightarrow \frac{d^2 u_{\pm}}{d\lambda^2} = \begin{cases} 0 & (|\lambda| > \epsilon) \\ -\kappa^2 u_{\pm} & (|\lambda| < \epsilon). \end{cases} \quad (5.13)$$

The equation (5.12) is easily solved under the initial conditions,

$$u_{\pm} = 0, \quad \frac{du_{\pm}}{d\lambda} = 1 \quad \text{at} \quad \lambda = -\lambda_0 < 0, \quad (5.14)$$

and we find the following properties under the condition that $\epsilon \sim \Delta\lambda/2 \ll \lambda_0 \sim R_i$.

F1 The case of $\epsilon\kappa \ll 1$

It corresponds to the case of E1. The bending angle, $\Delta\theta_{\pm}$, of the graph of C_{\pm} is well approximated as

$$\Delta\theta_{\pm} = \pm(\kappa\lambda_0)(2\kappa\epsilon) \sim \pm\kappa^2\lambda_0\Delta\lambda. \quad (5.15)$$

Note that $|\Delta\theta_{\pm}|$ can be larger than unity for the cases of large values of $\kappa\lambda_0 \sim \kappa R_i$.

F2 The case of $\epsilon\kappa > 1$

It corresponds to the case of E2. When light rays pass through the lens, u_{-} oscillates approximately $\epsilon\kappa/\pi$ times, while u_{+} exponentially grows as

$$\log u_{+} \sim \kappa\lambda + \log \left(\frac{1}{2} \lambda_0 e^{\epsilon\kappa} \right). \quad (5.16)$$

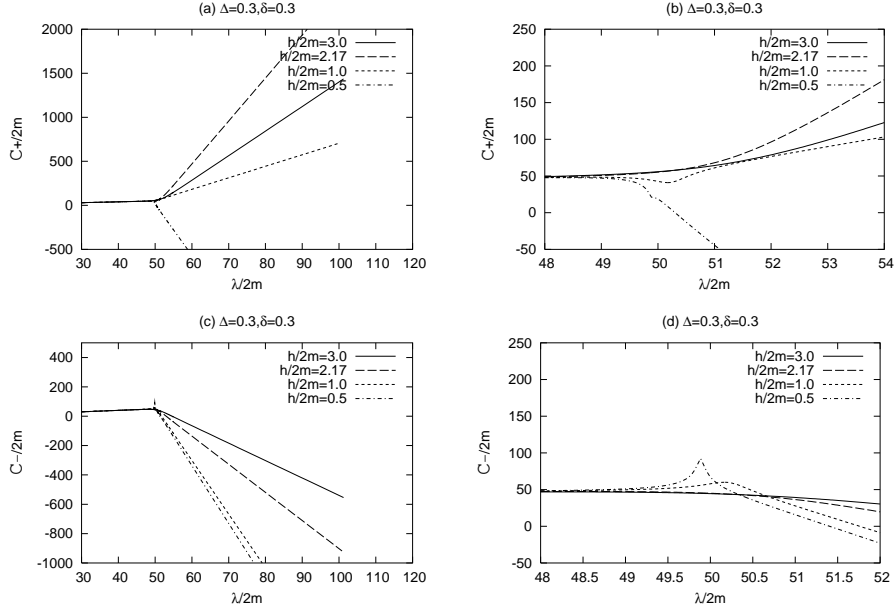


Fig. 13. We show (a) C_+ and (c) C_- as functions of λ for several values of the impact parameters, h , as denoted in each figure. The model parameters are chosen as those of the case [n_B], where $(\delta, \Delta) = (0.3, 0.3)$. The figures (b) and (d) are the enlarged parts of the figures (a) and (c), respectively.

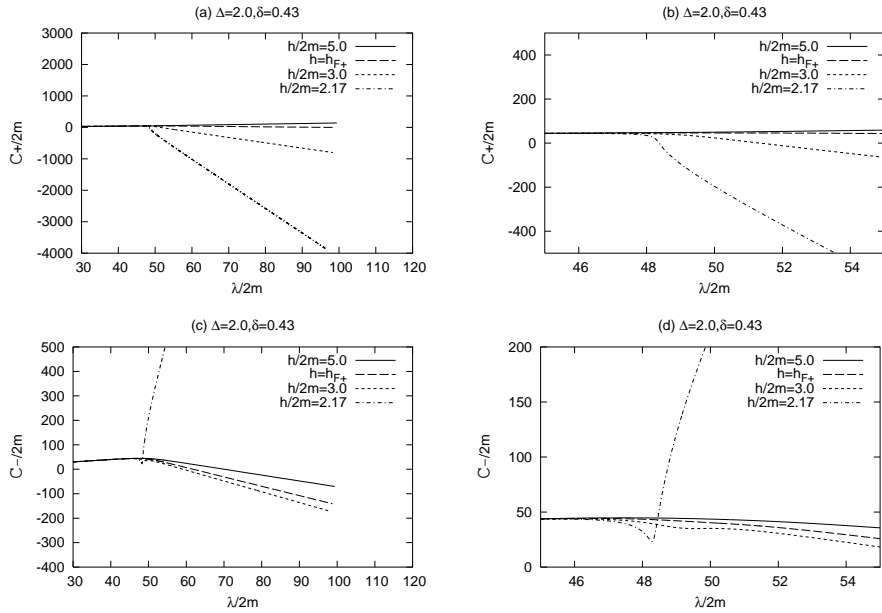


Fig. 14. We show (a) C_+ and (c) C_- as functions of λ for several values of the impact parameters, h , as denoted in each figure. The model parameters are chosen as those of the case [i], where $(\delta, \Delta) = (0.43, 2.0)$. The figures (b) and (d) are the enlarged parts of the figures (a) and (c), respectively.

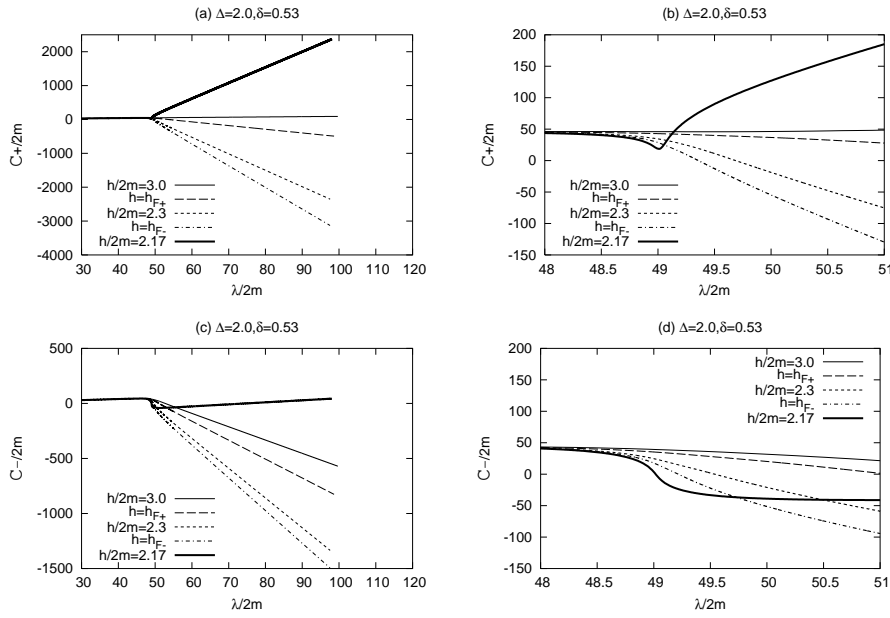


Fig. 15. We show (a) C_+ and (c) C_- as functions of λ for several values of the impact parameters, h , as denoted in each figure. The model parameters are chosen as those of the case [ii], where $(\delta, \Delta) = (0.53, 2.0)$. The figures (b) and (d) are the enlarged parts of the figures (a) and (c), respectively.

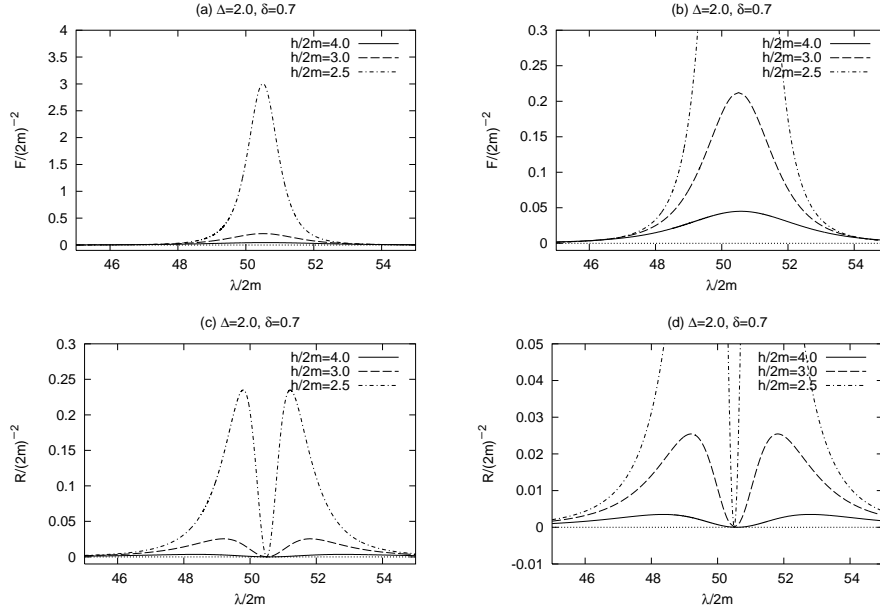


Fig. 16. We show the Weyl and Ricci source-terms, respectively, in the figures (a) and (c), as functions of the affine parameter, λ , for several values of the impact parameter, h . The model parameters are chosen as those of the case $[n_A]$, where $(\delta, \Delta) = (0.7, 2.0)$. The figures (b) and (d) are the enlarged central parts of the figures (a) and (c), respectively.

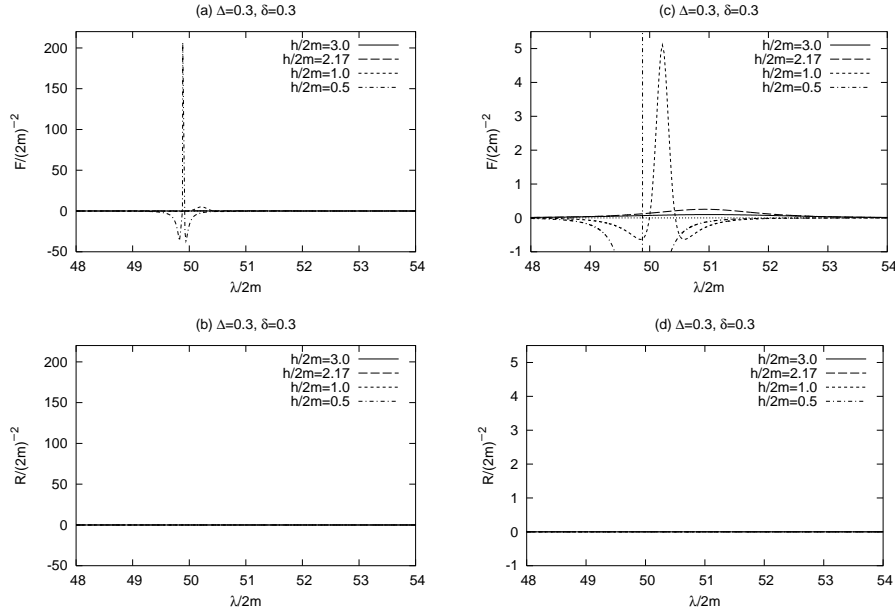


Fig. 17. We show the Weyl and Ricci source-terms, respectively, in the figures (a) and (c), as functions of the affine parameter, λ , for several values of the impact parameter, h . The model parameters are chosen as those of the case $[n_B]$: $(\delta, \Delta) = (0.3, 0.3)$. The figures (b) and (d) are the enlarged parts of the figures (a) and (c), respectively. The Ricci source-term, \mathcal{R} , is exactly zero for any value of h .

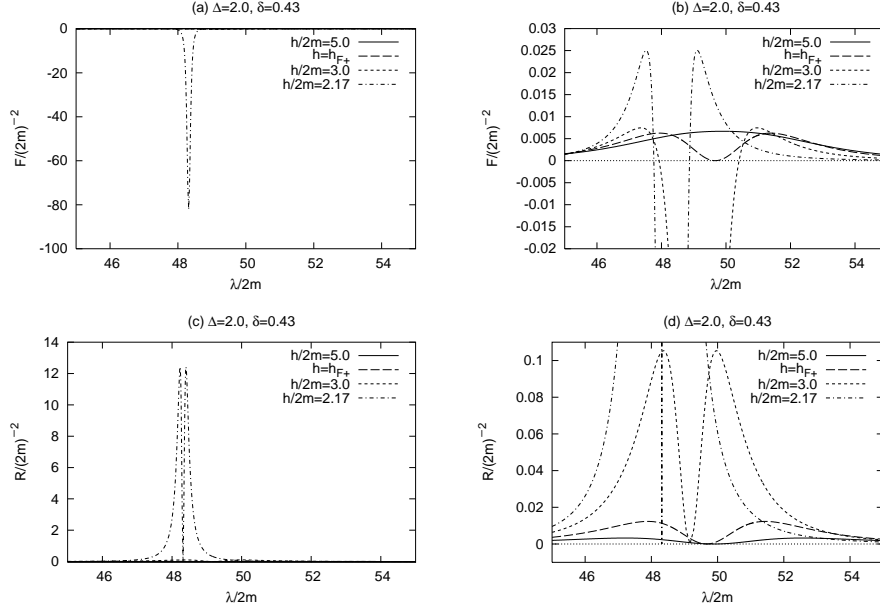


Fig. 18. We show the Weyl and Ricci source-terms, respectively, in the figures (a) and (c), as functions of the affine parameter, λ , for several values of the impact parameter, h . The model parameters are chosen as those of the case [i], where $(\delta, \Delta) = (2.0, 0.43)$. The figures (b) and (d) are the enlarged parts of the figures (a) and (c), respectively.

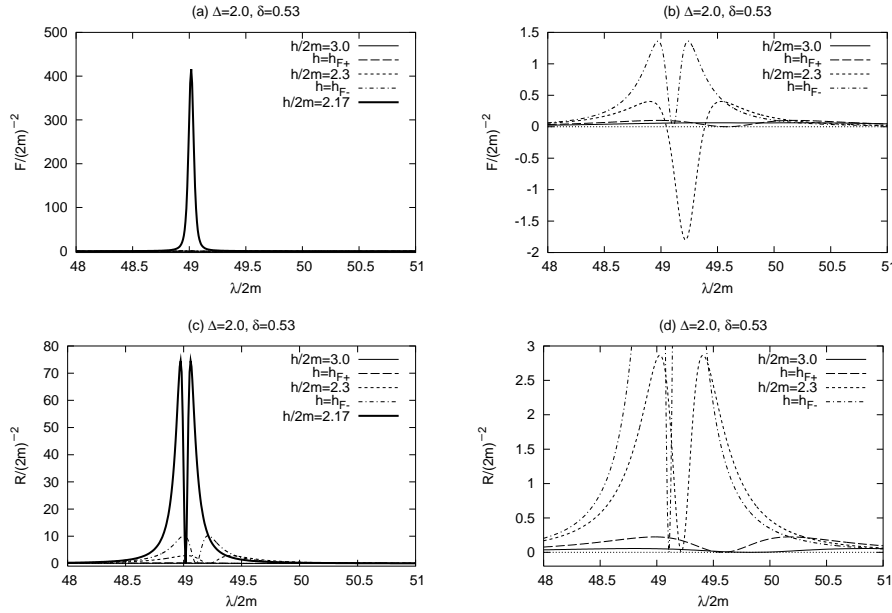


Fig. 19. We show the Weyl and Ricci source-terms, respectively, in the figures (a) and (c), as functions of the affine parameter, λ , for several values of the impact parameter, h . The model parameters are chosen as those of the case [ii], where $(\delta, \Delta) = (0.53, 2.0)$. The figures (b) and (d) are the enlarged parts of the figures (a) and (c), respectively.

The oscillatory properties of C_- have been expected by Dyer's results (see Appendix C), while we find that C_+ can oscillate because its combined source-term, $-\mathcal{R} + F$, can be negative not only in the scalar-tensor-Weyl solution but even in Voorhees's one. We have tried to find the numerical examples in which C_+ and C_- oscillate. After finely adjusting the model parameters, (δ, Δ) , and the impact parameter, h , we find several examples in which C_- oscillates. As for C_+ , however, we have failed. In Figure 20, we show the optical scalars, C_{\pm} , together with their source-terms for the case [ii] with $h/2m = 2.1609$. With Figures 20a and 20b, we obtain $\epsilon = 0.04 \times (2m)$ and $\kappa = 77/(2m)$ such that $\epsilon\kappa = 3.1 > 1$. We then estimate the expected number of times of the oscillations at $\epsilon\kappa/\pi \sim 1$, which is in accordance with the numerical one (see Figure 20f). As for C_+ , the analytic result (5.16) is approximate to the numerical one as follows,

$$\log C_{+}/2m \sim \begin{cases} 78\lambda/(2m) + 4 & \text{(Analytic)} \\ 80\lambda/(2m) + 6 & \text{(Numerical)}. \end{cases} \quad (5.17)$$

When the combined source-term has plural peaks, one can superpose the corresponding thin lenses.

Now we summarize the qualitative properties of C_+ and C_- along the light path for each region.

(N_A) In the region N_A, the Weyl source-term, F , is always dominant over the Ricci source-term, \mathcal{R} , and moreover is positive-definite. When the impact parameter is larger enough than m , the inequality, $\epsilon\kappa \ll 1$, holds, and the bending angle of the graph monotonously increases as the impact parameter decreases. Accordingly, there is a single caustic point, $h = h_a$, near the Einstein radius, h_E , such that C_- vanishes at the final time, $\lambda = \lambda_f$. For the smaller impact parameter, the inequality, $\epsilon\kappa > 1$, holds, and C_- can oscillate.

(N_B) In the region N_B, the Weyl source-term, F , is always dominant over the Ricci source-term, \mathcal{R} . When the impact parameter is large enough, the properties of C_+ and C_- are similar to those in the region N_A. For the smaller impact parameter, the Weyl source-term can be negative such that C_+ can decrease, while C_- can increase. Accordingly, there is a new caustic point, $h = h_b$, with $h_b = 3m \sim 6m$ such that C_+ vanishes at the final time. The intriguing thing for $h < h_b$ is that C_+ has negative values with the very large amplitude, while C_- is moderately positive. The case of C_- with $h/2m = 0.5$ may be an example of the superposition of triple lenses (see Figure 17a).

(I) In the region I, the Weyl source-term, F , is mostly dominant over the Ricci source-term, \mathcal{R} , and the Ricci-dominant cases are found only in the very narrow range of the impact parameter around h_{F+} . When $h_{F+} < h_E$, a first caustic point exists near h_E , and a second caustic points, $h = h_b$, appears near h_{F+} such that C_+ vanishes at the final time. It should be noted that the inequality, $h_{F+} < h_E$,

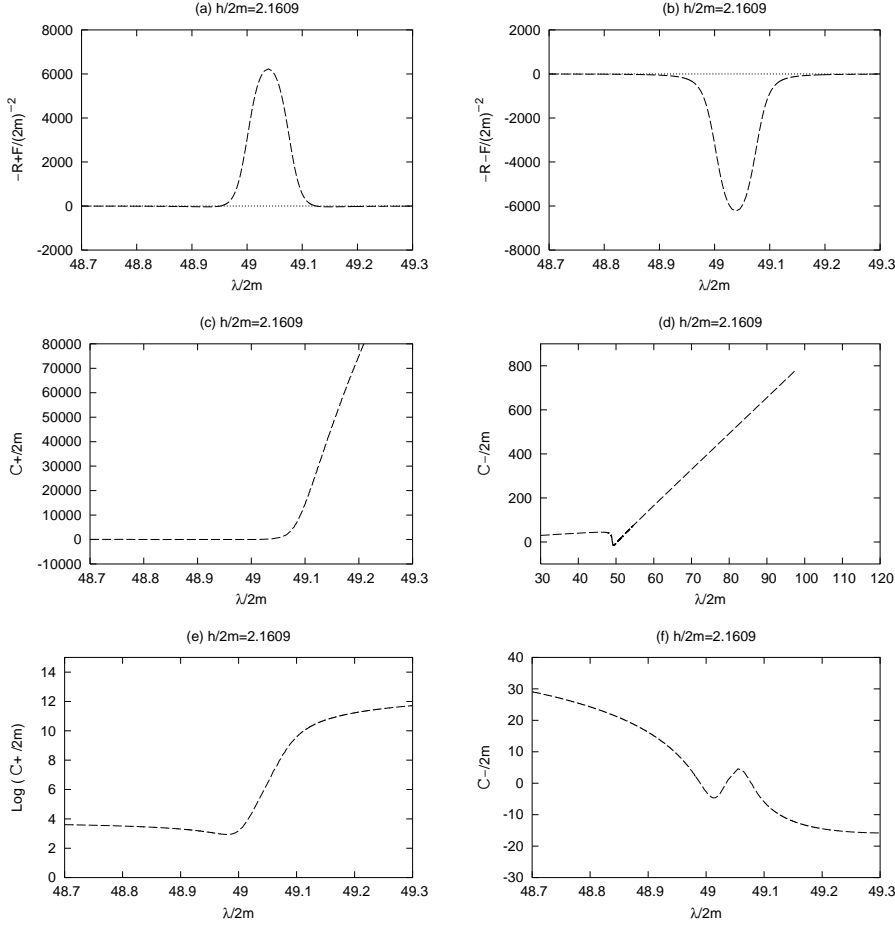


Fig. 20. In the case [ii], where $(\delta, \Delta) = (0.53, 2.0)$, we show (a) $-\mathcal{R} + F$, (b) $-\mathcal{R} - F$, (c) C_+ , (d) C_- and (e) $\log C_+$. The impact parameter, h , is finely adjusted as $h/2m = 2.1609$ such that C_- oscillates. The figure (f) is the enlarged part of the figure (d).

is easily violated in our numerical studies with $x_i = 100\delta$ (see Figure 23). In these cases, the caustic point, $h = h_b$, becomes the first one. Let C_+ and C_- at the final time, $\lambda = \lambda_f$, be functions of the impact parameter, h . For $h < h_b$, C_+ becomes negative with a larger amplitude for smaller h , while C_- changes its sign again and becomes positively larger for smaller h . Accordingly, a third caustic point can exist such that C_- vanishes at the final time.

(II) In the region II, the Weyl source-term, F , is mostly dominant over the Ricci source-term, \mathcal{R} , and the Ricci-dominant cases are found only in the very narrow ranges of the impact parameter around h_{F+} and h_{F-} . We find the very complicated structure of caustic points. For example, in the case [ii], we find four caustic points, h_a, h_b, h_c and h_d , where $h_a > h_b > h_c > h_d$ holds. The first caustic point, h_a , appears near the Einstein radius, h_E , such that C_- vanishes at the final time. The second and third ones, h_b and h_c , appear near h_{F+} and h_{F-} , respectively,

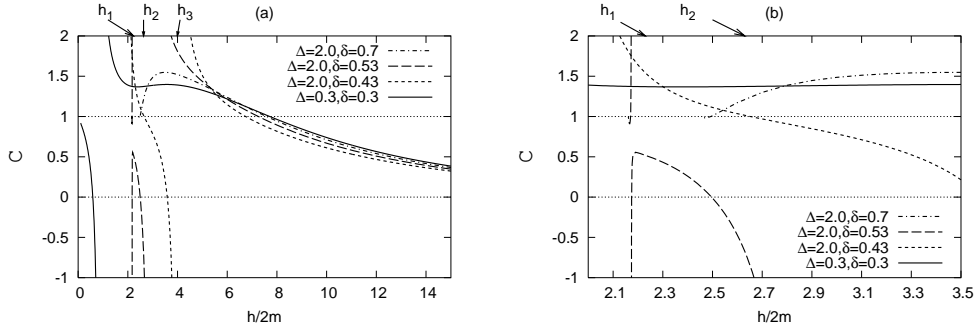


Fig. 21. In the figure (a), the image distortion rate, C , is shown as a function of the impact parameter, h . The model parameters are chosen to be the standard ones. The figure (b) is the enlarged part of the figure (a).

such that C_+ vanishes at the final time. Finally, the fourth one is associated with C_- such that C_- vanishes at the final time.

We have defined a conformally invariant variable, C , by $C = (C_+ - C_-)/C_+$, which can be interpreted as the image distortion rate. In Figure 21, we show C at the final time as a function of the impact parameter, h . As is noted above, one of the most intriguing properties of the graph is the appearance of the caustic points, and we find the following four cases of the number, N_+ , of the caustic points associated with C_+ :

- (a) $N_+ = 0$, (b) $N_+ = 1$, (c) $N_+ = 2$, (d) $N_+ \neq 0$ and $h_E < h_{F+}$.

Now we should remind ourselves that h_E is an extrinsic scale including the initial distance to the source, $R_i = R_x(x_i)$. It is naturally expected that the cases of (d) are distributed to (b) and (c). As such an example, we investigate the cases of $(\delta, \Delta) = (2.0, 0.3)$ in the region I and $(\delta, \Delta) = (4.0, 0.6)$ in the region II. In both cases, we have $h_{F+}/2m > h_E/2m \sim 7$ for $x_i = 100\delta$ and $h_{F+}/2m < h_E/2m \sim 14$ for $x_i = 400\delta$. We show the image distortion rate, C , as a function of the impact parameter, h , in Figure 22. The graphs show the “anomalies” for the cases of $x_i = 100\delta$ in the sense that the first caustic point, $C = 1$, near the Einstein radius, h_E , disappears. That is, a naked caustic point associated with C_+ appears near h_{F+} . For the cases of $x_i = 400\delta$, this anomalous caustic point is hidden by the Einstein radius, h_E , such that the first caustic point appears near h_E as the one associated with C_- . We classify the parameter space, (δ, Δ) , on the basis of the above conditions, (a)~(d), as is depicted in Figure 23. Again, we find a close relationship between the above new classification and the previous one.

We summarize the relationship between our numerical results and the classification of the parameter space, (δ, Δ) , in Table I.

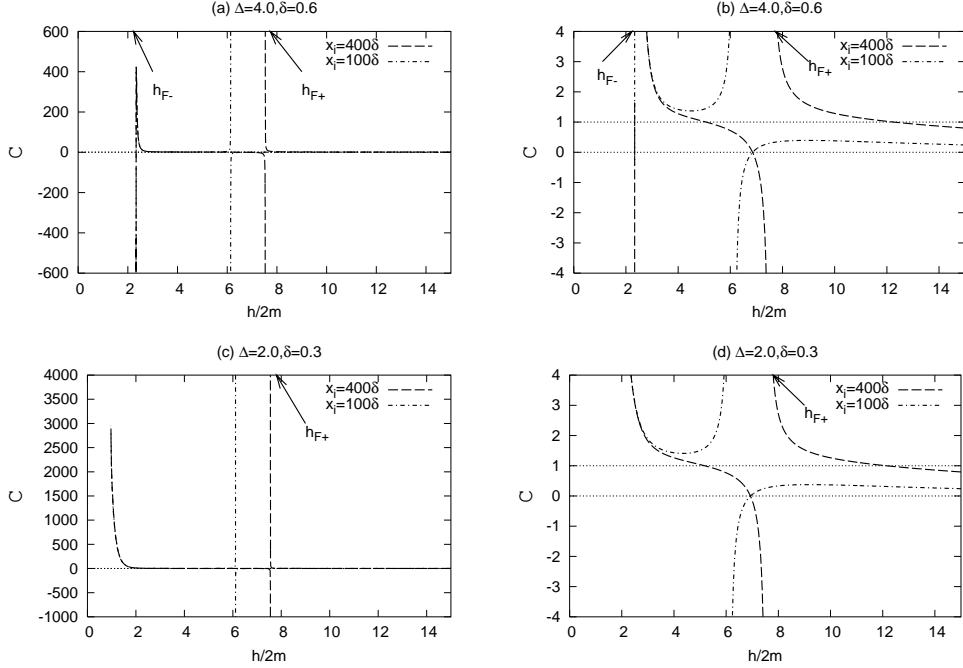


Fig. 22. We show the image distortion rate, C , as a function of the impact parameter, h , for two cases: (a) $(\delta, \Delta) = (0.6, 4.0)$ in the region II and (c) $(\delta, \Delta) = (0.3, 2.0)$ in the region I. The enlarged figures (b) and (d) correspond to the figures (a) and (c), respectively.

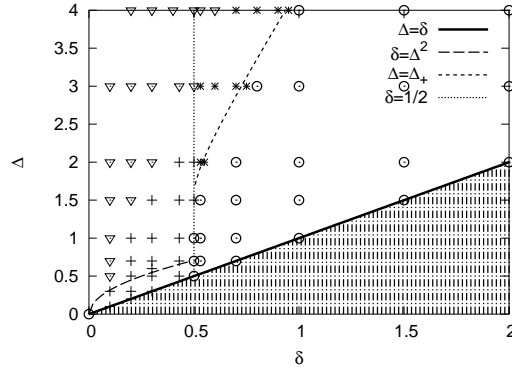


Fig. 23. We classify the parameter space, (δ, Δ) , into the four groups, (a)~(d), on the basis of the number of the caustic points, N_+ , associated with C_+ , as is explained in the text: (a) an open circle, (b) +, (c) * and (d) a reversed triangle.

Table I. The classification of the parameter space, (δ, Δ)

| Classification of $F(x_o)$ | N_A | N_B | I | II | Fig. 3 |
|--------------------------------------|--------------|-------|---|----------|---------|
| Reflecting region | mostly blank | + | + | + | Fig. 7 |
| Extremes of the deflection angle | mostly blank | + | + | * | Fig. 10 |
| Negative deflection angle | blank | • | • | mostly • | Fig. 11 |
| Caustic points associated with C_+ | mostly ○ | + | + | * | Fig. 23 |

§6. A closing remark

In this paper, we have investigated several properties of null geodesics and null geodesic congruences with the aim of finding the crucial, experimentally detectable difference between the theory of general relativity and scalar-tensor theories of gravity. Our studies are very restricted ones because they are performed only for specific null geodesics (ones on the equatorial plane, $y = 0$) with a specific solution (the scalar-tensor-Weyl solution). These specific null geodesics may be unstable when there are additional small fluctuations, especially those in the y -direction. One may doubt the realities of the specific solution as a mathematical model of the spacetime. Indeed we cannot guarantee its realities. Nevertheless, we would like to claim that we have succeeded in discovering the new world, namely the region II in the classified parameter space. The lensing properties found in this region are never seen in the other regions, N_A , N_B and I. Unfortunately, the border between the region II (the new world) and the region N_A (the Einstein-like world) is rather vague, and moreover, the most precious things (h_{F+} and h_{F-}) may be hidden by the Einstein radius, h_E . But one will go there: *someday, somewhere, somehow*.¹⁵⁾

Acknowledgements We would like to thank Ken-ichi Oohara and Ryoichi Nishi for helpful comments.

Appendix A

— The Ernst-like equations in scalar-tensor theories —

In the stationary, axisymmetric spacetime, there exist two Killing vectors, $\xi = \partial_t$ and $\eta = \partial_\phi$. It is shown that the energy-momentum tensor, $T^{\alpha\beta}$, of the Maxwell fields satisfies the following relations,¹²⁾

$$\xi^\alpha T_\alpha^{[\beta} \xi^\gamma \eta^{\delta]} = \eta^\alpha T_\alpha^{[\beta} \xi^\gamma \eta^{\delta]} = 0. \quad (\text{A}\cdot 1)$$

One finds that the similar relations hold for $S_{\mu\nu} \equiv 2\partial_\mu\varphi\partial_\nu\varphi$, accordingly, with Theorem 7.1.1 in Ref.13, the metric of the Einstein-Maxwell system with a scalar field, φ , can be reduced to the following form,

$$ds^2 = -e^{2\psi}(dt - \omega d\phi)^2 + e^{-2\psi} [e^{2\gamma}(d\rho^2 + dz^2) + \rho^2 d\phi^2], \quad (\text{A}\cdot 2)$$

where the metric functions, ψ , γ and ω , are functions of $x^1 \equiv \rho$ and $x^2 \equiv z$.

After long and complicated calculations, one finds that the field equations are reduced to the following set of equations,

$$e^{2\psi} = \frac{1}{2} (\mathcal{E} + \bar{\mathcal{E}}) + \Phi\bar{\Phi}, \quad (\text{A}\cdot 3\text{a})$$

$$e^{2\psi}\nabla^2\mathcal{E} = (\nabla\mathcal{E}) \cdot [(\nabla\mathcal{E}) + 2\bar{\Phi}\nabla\Phi], \quad (\text{A}\cdot 3\text{b})$$

$$e^{2\psi}\nabla^2\bar{\Phi} = (\nabla\bar{\Phi}) \cdot [(\nabla\mathcal{E}) + 2\bar{\Phi}\nabla\Phi], \quad (\text{A}\cdot 3\text{c})$$

$$\begin{aligned} \gamma_{,1} = & \rho [(\psi_{,1})^2 - (\psi_{,2})^2] - \frac{1}{4\rho} [(\omega_{,1})^2 - (\omega_{,2})^2] e^{4\psi} \\ & - \rho(\Phi_{,1}\bar{\Phi}_{,1} - \Phi_{,2}\bar{\Phi}_{,2})e^{-2\psi} + \rho [(\varphi_{,1})^2 - (\varphi_{,2})^2], \end{aligned} \quad (\text{A}\cdot\text{3d})$$

$$\gamma_{,2} = 2\rho\psi_{,1}\psi_{,2} - \frac{1}{2\rho}\omega_{,1}\omega_{,2}e^{4\psi} - \rho(\Phi_{,1}\bar{\Phi}_{,2} + \Phi_{,2}\bar{\Phi}_{,1})e^{-2\psi} + 2\rho\varphi_{,1}\varphi_{,2}, \quad (\text{A}\cdot\text{3e})$$

$$\nabla^2\varphi = 0, \quad (\text{A}\cdot\text{3f})$$

where, for any functions, f and h ,

$$\nabla^2 f \equiv \frac{1}{\rho} \frac{\partial}{\partial \rho} \left(\rho \frac{\partial f}{\partial \rho} \right) + \frac{\partial^2 f}{\partial z^2}, \quad \nabla f \cdot \nabla h \equiv \frac{\partial f}{\partial \rho} \frac{\partial h}{\partial \rho} + \frac{\partial f}{\partial z} \frac{\partial h}{\partial z}, \quad f_{,i} \equiv \frac{\partial f}{\partial x^i}. \quad (\text{A}\cdot\text{4})$$

In Ref.14, there are explicit forms of the metric function, ω , and the Maxwell fields in terms of the complex potentials, \mathcal{E} and Φ . One notes that the equations (A.3a)~(A.3c) are the same as those in general relativity and are referred to as the Ernst equations of the Einstein-Maxwell system. The remaining equations contain the scalar field contributions, and, as for the metric functions, effects of the scalar field appear only in γ .

Appendix B

— The scalar-tensor-Weyl solution —

In the case of static, axisymmetric vacuum solutions, one has $\omega = \Phi = 0$, and the field equations (A.3a)~(A.3f) become the following set of equations,

$$e^{2\psi} = \mathcal{E}, \quad (\text{B}\cdot\text{1a})$$

$$\mathcal{E}\nabla^2\mathcal{E} = (\nabla\mathcal{E}) \cdot (\nabla\mathcal{E}), \quad (\text{B}\cdot\text{1b})$$

$$\gamma_{,1} = \rho [(\psi_{,1})^2 - (\psi_{,2})^2] + \rho [(\varphi_{,1})^2 - (\varphi_{,2})^2], \quad (\text{B}\cdot\text{1c})$$

$$\gamma_{,2} = 2\rho\psi_{,1}\psi_{,2} + 2\rho\varphi_{,1}\varphi_{,2}, \quad (\text{B}\cdot\text{1d})$$

$$\nabla^2\varphi = 0, \quad (\text{B}\cdot\text{1e})$$

where \mathcal{E} is a real function. One finds that the equation for ψ is reduced to

$$\nabla^2\psi = 0. \quad (\text{B}\cdot\text{2})$$

That is, φ and ψ are harmonic functions.

We introduce *oblate* and *prolate* coordinates, (x, y) , defined by

$$\rho = \sigma\sqrt{(x^2 + \epsilon)(1 - y^2)}, \quad (\text{B}\cdot\text{3a})$$

$$z = \sigma xy, \quad (\text{B}\cdot\text{3b})$$

where σ is a positive constant, and $\epsilon = \pm 1$. The cases, $\epsilon = 1$ and $\epsilon = -1$, are referred to as *oblate* and *prolate*, respectively. The equation (B.2) is then reduced to

$$\frac{\partial}{\partial x} \left[(x^2 + \epsilon) \frac{\partial \psi}{\partial x} \right] + \frac{\partial}{\partial y} \left[(1 - y^2) \frac{\partial \psi}{\partial y} \right] = 0. \quad (\text{B}\cdot\text{4})$$

A similar equation holds for φ .

The simplest prolate solution for ψ is given by

$$\psi = \frac{\delta}{2} \ln \left(\frac{x-1}{x+1} \right), \quad (\text{B}\cdot\text{5})$$

where δ is an integration constant. A similar solution for φ is given by

$$\varphi = \varphi_0 + \frac{d}{2} \ln \left(\frac{x-1}{x+1} \right), \quad (\text{B}\cdot\text{6})$$

where φ_0 and d are integration constants. Then the corresponding metric function, γ , becomes

$$e^{2\gamma} = \left(\frac{x^2-1}{x^2-y^2} \right)^{\Delta^2}, \quad (\text{B}\cdot\text{7})$$

where

$$\Delta^2 \equiv \delta^2 + d^2. \quad (\text{B}\cdot\text{8})$$

For completeness, we give an explicit form of the metric:

$$ds^2 = - \left(\frac{x-1}{x+1} \right)^\delta dt^2 + \sigma^2 \left(\frac{x-1}{x+1} \right)^{-\delta} \times \left[\left(\frac{x^2-1}{x^2-y^2} \right)^{\Delta^2} (x^2-y^2) \left(\frac{dx^2}{x^2-1} + \frac{dy^2}{1-y^2} \right) + (x^2-1)(1-y^2)d\phi^2 \right]. \quad (\text{B}\cdot\text{9})$$

One notes that, though ψ and φ are independent of y , γ depends on both x and y .

Appendix C

— Analytic solutions to the optical scalar equations —

C.1. Static, spherically symmetric spacetime

We summarize the analytic results obtained by Dyer.¹¹⁾ A metric of the static, spherically symmetric spacetime is given by

$$ds^2 = -e^{2C} dt^2 + e^{2A} dr^2 + e^{2B} d\Omega^2, \quad (\text{C}\cdot\text{1})$$

where A , B and C are functions of r . A null vector, k^μ , which is tangent to the null geodesic in this spacetime, is obtained as

$$\begin{aligned} k^0 &= e^{-2C}, \quad k^2 = 0, \quad k^3 = h e^{-2B}, \\ k^1 &= \pm e^{-(A+C)} \sqrt{1 - h^2 e^{2(C-B)}}, \end{aligned} \quad (\text{C}\cdot\text{2})$$

where a constant, h , is an impact parameter, and we assume that the geodesic is on the equatorial plane, $\theta = \pi/2$, without loss of generality. The complex null vector,

t^μ , becomes

$$\begin{aligned} t^0 &= \frac{e^{-C}}{2\sqrt{2}} \left[\frac{2}{h} S_+ S_- e^B + H(S_+^2 + S_-^2) \right], \quad t^2 = \frac{i}{\sqrt{2}} e^{-B}, \\ t^1 &= \frac{e^{-A}}{2\sqrt{2}} \left[\frac{1}{h} (S_+^2 + S_-^2) e^B + 2HS_+ S_- \right], \quad t^3 = \frac{Hh}{\sqrt{2}} e^{-2B}, \\ S_\pm &= \sqrt{e^{-C} \pm h e^{-B}}, \quad H = -\frac{1}{h} \int^r \frac{B'}{S_+ S_-} e^{B-C} dr, \end{aligned} \quad (\text{C.3})$$

where a prime denotes a differentiation with respect to r . Then the Ricci and Weyl source-terms, \mathcal{R} and F , in (4.17) and (4.18) are evaluated as

$$\begin{aligned} -\mathcal{R} + F &= e^{-2(A+C)} (B'' + (B')^2 - B'C' - B'A') \\ &\quad - h^2 e^{-2(A+B)} (C'' + (C')^2 - C'B' - C'A'), \\ -\mathcal{R} - F &= e^{-2(A+C)} (B'' + (B')^2 - B'C' - B'A') \\ &\quad - h^2 e^{-2(A+B)} (e^{2(A-B)} + B'' - A'B'). \end{aligned} \quad (\text{C.4})$$

Since the Weyl source-term, F , is real, one can let the shear, σ , be real without loss of generality. Dyer has introduced the new optical scalars, C_\pm , defined by

$$\frac{d}{d\lambda} \ln C_\pm = \theta \pm \sigma, \quad (\text{C.5})$$

and has obtained the following equations,

$$\frac{d^2 C_\pm}{d\lambda^2} = (-\mathcal{R} \pm F) C_\pm. \quad (\text{C.6})$$

General solutions to (C.6) are given as

$$\begin{aligned} C_+ &= C_+^0 \sqrt{e^{2B} - h^2 e^{2C}} \left\{ \int^r \frac{e^{A+B+C}}{[e^{2B} - h^2 e^{2C}]^{\frac{3}{2}}} dr + D_+^0 \right\}, \\ C_- &= C_-^0 e^B \sin \left(h \int^r \frac{e^{A-B+C}}{\sqrt{e^{2B} - h^2 e^{2C}}} dr + D_-^0 \right), \end{aligned} \quad (\text{C.7})$$

where C_\pm^0 and D_\pm^0 are integration constants.

C.2. Static, axisymmetric spacetime

A metric of the static, axisymmetric spacetime is given by

$$ds^2 = -e^{2\alpha} dt^2 + e^{2\beta} dx^2 + e^{2\gamma} dy^2 + e^{2\mu} d\phi^2, \quad (\text{C.8})$$

where the metric functions, α , β , γ and μ are functions of x and y . A null vector, k^μ , which is tangent to the null geodesic on the equatorial plane, $y = 0$, is obtained as

$$\begin{aligned} k^0 &= e^{-2\alpha}, \quad k^2 = 0, \quad k^3 = h e^{-2\mu}, \\ k^1 &= \pm e^{-\beta} \sqrt{e^{-2\alpha} - h^2 e^{-2\mu}}, \end{aligned} \quad (\text{C.9})$$

where a constant, h , is an impact parameter. The complex null vector, t^μ , becomes

$$\begin{aligned}
 t^0 &= \frac{1}{2\sqrt{2}} \left[\frac{2}{h} e^\mu S_+ S_- + H(S_+^2 + S_-^2) \right] e^{-\alpha}, & t^2 &= \frac{i}{\sqrt{2}} e^{-\gamma}, \\
 t^1 &= \frac{1}{2\sqrt{2}} \left[\frac{1}{h} (S_+^2 + S_-^2) e^\mu + 2H S_+ S_- \right] e^{-\beta}, & t^3 &= \frac{1}{\sqrt{2}} H h e^{-2\mu}, \\
 S_\pm &= \sqrt{e^{-\alpha} \pm h e^{-\mu}}, & H &= -\frac{1}{h} \int^x \frac{e^{\mu-\alpha}}{S_+ S_-} \frac{\partial \mu}{\partial x} dx.
 \end{aligned} \tag{C-10}$$

References

- 1) C. Brans and R. H. Dicke, *Phys. Rev.* **124** (1962), 925.
- 2) M. B. Green, J. H. Schwartz and E. Witten, *Superstring Theory vols. 1, 2*, (Cambridge University Press, Cambridge, 1987).
- 3) T. Damour and G. Esposito-Farèse, *Class. Quant. Grav.* **9**, (1992), 2093 .
- 4) T. Damour and G. Esposito-Farèse, *Phys. Rev. Lett.* **70** (1993), 2220.
- 5) T. Damour and G. Esposito-Farèse, *Phys. Rev. D* **54** (1996), 1474 .
- 6) T. Tsuchida, G. Kawamura and K. Watanabe, *Prog. Theor. Phys.* **100** (1998), 291.
- 7) T. Tsuchida and K. Watanabe, *Prog. Theor. Phys.* **101** (1999), 73.
- 8) A. Tomimatsu and H. Sato, *Prog. Theor. Phys.* **50** (1972), 95.
- 9) B. Voorhees, *Phys. Rev. D* **2** (1970), 2119.
- 10) R. K. Sachs, *Proc. R. Soc. London*, **A264**, (1961), 309.
- 11) C. C. Dyer, *Mon. Not. R. Astr. Soc.*, **180**, (1977), 231.
- 12) B. Carter, *J. Math. Phys.* **10** (1969), 70.
- 13) R. M. Wald, *General Relativity*, (The University of Chicago Press, Chicago and London, 1984).
- 14) S. Chandrasekhar, *The Mathematical Theory of Black Holes* (Oxford University Press, New York, 1983).
- 15) *A passage from some famous song.*